

# Kitaev Materials

Simon Trebst

Institute for Theoretical Physics

University of Cologne, 50937 Cologne, Germany

## Contents

<b>1</b>	<b>Spin-orbit entangled Mott insulators</b>	<b>2</b>
1.1	Bond-directional interactions . . . . .	4
1.2	Kitaev model . . . . .	6
<b>2</b>	<b>Honeycomb Kitaev materials</b>	<b>9</b>
2.1	$\text{Na}_2\text{IrO}_3$ . . . . .	9
2.2	$\alpha\text{-Li}_2\text{IrO}_3$ . . . . .	10
2.3	$\alpha\text{-RuCl}_3$ . . . . .	11
<b>3</b>	<b>Triangular Kitaev materials</b>	<b>15</b>
3.1	$\text{Ba}_3\text{Ir}_x\text{Ti}_{3-x}\text{O}_9$ . . . . .	15
3.2	Other materials . . . . .	17
<b>4</b>	<b>Three-dimensional Kitaev materials</b>	<b>17</b>
4.1	Conceptual overview . . . . .	18
4.2	$\beta\text{-Li}_2\text{IrO}_3$ and $\gamma\text{-Li}_2\text{IrO}_3$ . . . . .	22
4.3	Other materials . . . . .	23
<b>5</b>	<b>Outlook</b>	<b>24</b>

## 1 Spin-orbit entangled Mott insulators

Transition-metal oxides with partially filled  $4d$  and  $5d$  shells exhibit an intricate interplay of electronic, spin, and orbital degrees of freedom arising from a largely accidental balance of electronic correlations, spin-orbit entanglement, and crystal-field effects [1]. With different materials exhibiting slight tilts towards one of the three effects, a remarkably broad variety of novel forms of quantum matter can be explored. On the theoretical side, topology is found to play a crucial role in these systems – an observation which, in the weakly correlated regime, has lead to the discovery of the topological band insulator [2, 3] and subsequently its metallic cousin, the Weyl semi-metal [4, 5]. Upon increasing electronic correlations, Mott insulators with unusual local moments such as spin-orbit entangled degrees of freedom can form and whose collective behavior gives rise to unconventional types of magnetism including the formation of quadrupolar correlations or the emergence of so-called spin liquid states. A rough guide to these novel types of quantum matter, currently widely explored in materials with substantial spin-orbit coupling, is given by the general phase diagram of Fig. 1, adapted from an early review [6] of this rapidly evolving field at the current forefront of condensed matter physics.

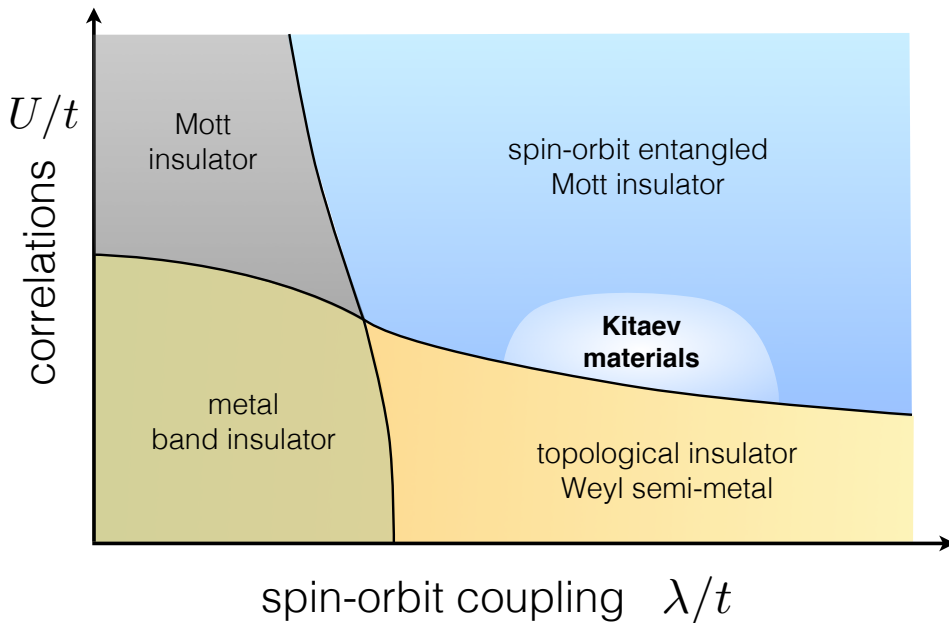


**Fig. 1:** General form of the phase diagram in the presence of electronic correlations and spin-orbit coupling. Figure adapted from the review [6].

Our focus here will be on the particularly intriguing scenario of the formation of novel types of Mott insulators in which the local moments are spin-orbit entangled  $j = 1/2$  Kramers doublets [7, 8, 9]. The latter are formed for ions in a  $d^5$  electronic configuration – a vast family of such  $d^5$  materials exists that not only includes most iridates, which typically have a  $\text{Ir}^{4+}$  ( $5d^5$ ) valence, but also some Ru-based materials with a  $\text{Ru}^{3+}$  ( $4d^5$ ) valence along with the (extremely toxic) osmates and (so far largely unexplored) rhenates. The level scheme of such  $d^5$  ionic systems is illustrated in Fig. 2. With the crystal field (e.g. of an octahedral oxygen cage) splitting off the two  $e_g$  levels, this puts the five electrons with a total  $s = 1/2$  magnetic moment into the  $t_{2g}$  orbitals with an effective  $\ell = 1$  orbital moment. Strong spin-orbit coupling then results in a system with a fully filled  $j = 3/2$  band and a half-filled  $j = 1/2$  band. The reduced bandwidth

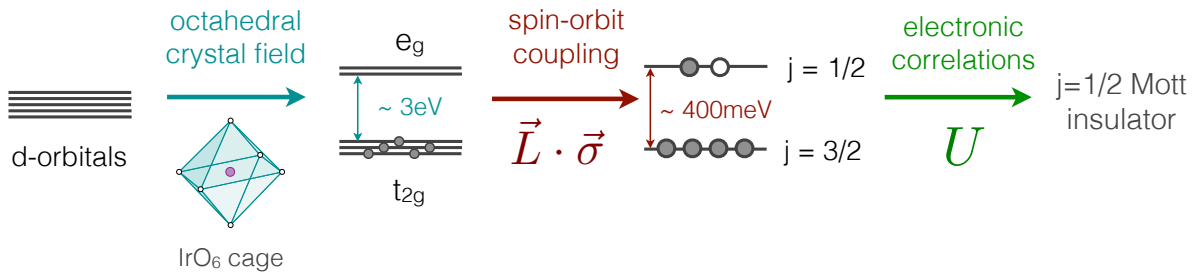


**Fig. 2:** Formation of spin-orbit entangled  $j = 1/2$  moments for ions in a  $d^5$  electronic configuration such as for the typical iridium valence  $\text{Ir}^{4+}$  or the ruthenium valence  $\text{Ru}^{3+}$ .

of the latter then allows for the opening of a Mott gap even for the relatively moderate electronic correlations of the 4d and 5d compounds. This latter point should again be emphasized. The formation of a Mott insulator in these compounds is *per se* somewhat counterintuitive as the larger atomic radii of their 4d and 5d constituents give rise to considerable atomic overlap, which results in a large electronic bandwidth and thus an effective suppression of the electronic correlations. As such, conventional wisdom has long considered these “heavy” transition metal compounds to generically form metallic states. It is only because of an enormously enhanced spin-orbit coupling that the effective electronic bandwidth of these materials can be reduced (via the formation of two separate  $j = 3/2$  and  $j = 1/2$  bands) to a level that the largely suppressed electronic correlations can still drive the system into a Mott insulating state. These  $j = 1/2$  Mott materials are therefore sometimes referred to as “spin-orbit assisted Mott insulators” and are located in the proximity of the metal-insulator transition for large spin-orbit coupling in the general phase diagram of Fig. 1.

The formation of such a  $j = 1/2$  Mott insulator was first observed experimentally in 2008/2009 [10, 11] for the perovskite iridate  $\text{Sr}_2\text{IrO}_4$  – a 5d transition-metal oxide which is an isostructural analogue of  $\text{La}_2\text{CuO}_4$ , the parent compound of the cuprate superconductors. Remarkably, its low-temperature physics indeed shares a striking resemblance to the phenomenology of the cuprate superconductors including the formation of long-range antiferromagnetic order of the  $j = 1/2$  pseudospins for the undoped material and the emergence of a pseudogap phase and associated Fermi arcs for electron-doped systems [12, 13, 14]. There is an intense ongoing search [15, 16] for superconductivity in  $\text{Sr}_2\text{IrO}_4$  and other perovskite iridates.

In parallel, much attention has been drawn towards  $j = 1/2$  Mott insulators that exhibit bond-directional exchange interactions and are thought to exhibit unconventional forms of magnetism, such as the emergence of spin liquids [17, 18] or the formation of non-trivial spin textures. We refer to these systems as *Kitaev materials*. Of particular interest here are the sister compounds  $\text{Na}_2\text{IrO}_3$  and  $\alpha\text{-Li}_2\text{IrO}_3$  and more recently  $\alpha\text{-RuCl}_3$  that form Mott insulators, in which local  $j = 1/2$  moments are aligned in (almost decoupled) hexagonal layers. As such they are perfect candidate materials for a solid-state realization of the Kitaev honeycomb model [19] as envisioned by Jackeli and Khaliullin in 2009 [9]. Over the last few years, materials synthesis of novel  $j = 1/2$  Mott insulators has been thriving at a remarkable pace and has further broadened our view on Kitaev materials beyond the original honeycomb structure. As will be outlined in the remainder of this chapter,  $j = 1/2$  Mott insulators with strong bond-directional exchange interactions have also been synthesized for triangular lattice geometries, e.g. in the family of hexagonal perovskites  $\text{Ba}_3\text{Ir}_x\text{Ti}_{3-x}\text{O}_9$ , and three-dimensional, tricoordinated lattice generalizations of the honeycomb lattice (dubbed the hyper-honeycomb

and stripy-honeycomb) in polymorphs of  $\alpha\text{-Li}_2\text{IrO}_3$ , i.e. the iridates  $\beta\text{-Li}_2\text{IrO}_3$  and  $\gamma\text{-Li}_2\text{IrO}_3$ , respectively. In addition, theoretical progress has been made in comprehensively classifying the gapless spin liquid ground states of three-dimensional Kitaev models. It will be the purpose of this chapter to provide what is hopefully a concise review of the current status of these Kitaev materials and their conceptual understanding.

## 1.1 Bond-directional interactions

At the heart of all Kitaev materials are bond-directional interactions, i.e. Ising-like interactions where the exchange easy axis depends on the spatial orientation of an exchange bond, and which dominate in coupling strength over all other exchange types. The microscopic origin of such bond-directional interactions in  $d^5$  transition metal compounds has been worked out in a pioneering 2005 paper by Khaliullin [7] and later refined to the context of Kitaev-type interactions in joint work of Jackeli and Khaliullin [9]. These papers have undoubtedly shaped the formation of what is now a burgeoning field of experimental and theoretical exploration of Kitaev materials.

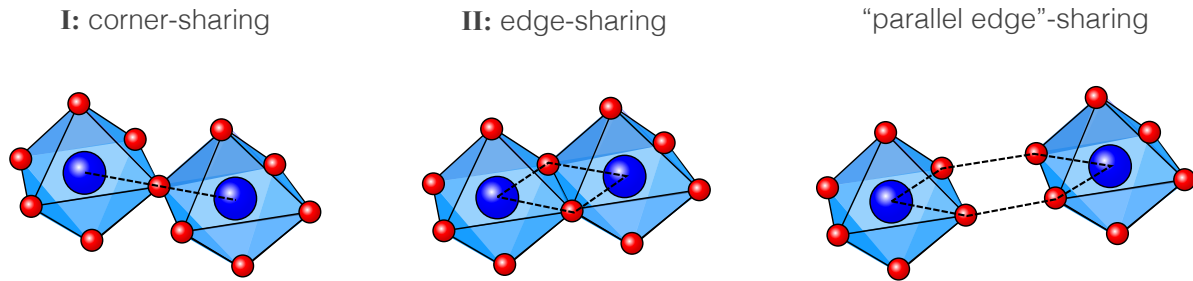


**Fig. 3:** Illustration of possible geometric orientations of neighboring  $\text{IrO}_6$  octahedra that give rise to different types of (dominant) exchange interactions between the magnetic moments located on the iridium ion at the center of these octahedra. For the corner-sharing geometry (I) one finds a dominant symmetric Heisenberg exchange, while for the edge-sharing geometries (II) one finds a dominant bond-directional, Kitaev-type exchange.

What Khaliullin and Jackeli have realized is that the geometric orientation of neighboring  $\text{IrO}_6$  octahedra plays a crucial role in determining the microscopic exchange of the magnetic moments located on the iridium ion at the center of these octahedra. They distinguish two elementary scenarios, which are illustrated (along with an extension) in Fig. 3. First, for perovskite iridates such as  $\text{Sr}_2\text{IrO}_4$  two neighboring  $\text{IrO}_6$  octahedra share a *corner*. For the coupling between the two neighboring iridium ions this means that there is a single  $\text{Ir}-\text{O}-\text{Ir}$  exchange path, which is also referred to as  $180^\circ$  bond. The dominant coupling along this type of bond is – despite the presence of a strong spin-orbit coupling – a symmetric Heisenberg exchange between the spin-orbit entangled  $j = 1/2$  moments. The second scenario plays out in materials, in which two neighboring  $\text{IrO}_6$  octahedra share an *edge*. Here there are two  $\text{Ir}-\text{O}-\text{Ir}$  exchange paths, which exhibit a  $90^\circ$  bonding geometry. The fact that there are *two* exchange paths turns out to be crucial, as the two alternative paths lead to a destructive interference of the symmetric Heisenberg exchange when restricting the coupling to arise exclusively from the  $j = 1/2$  bands, or alternatively to a significant suppression to some residual Heisenberg exchange when considering the full multi-orbital model also including the (virtual)  $j = 3/2$  bands. In lieu of the highly suppressed isotropic exchange, it is a bond-directional coupling, stemming from Hund's

coupling and mediated through the multiplet structure of the excited levels, that takes center stage and becomes the dominant coupling. The bond-directionality of the coupling arises since the pair of  $d$ -orbitals linked for two neighboring octahedra depends on the type of edge shared at their intersection. This in turn gives rise to a spatially oriented Ising-type coupling between the spin-orbit entangled  $j = 1/2$  moments where the magnetic easy-axis is perpendicular to the plane spanned by the two exchange paths [7, 9]. The strength of this bond-directional coupling is given by

$$-\frac{8t^2 J_H}{3U^2} S_1^\gamma S_2^\gamma, \quad (1)$$

where  $t$  is the effective interorbital hopping mediated by the oxygen ions,  $J_H$  is the Hund's coupling and  $U$  the electronic correlation strength. The two spin-orbit entangled  $j = 1/2$  moments, represented by the usual vectors of SU(2) spin-1/2 Pauli matrices  $\mathbf{S}_1$  and  $\mathbf{S}_2$ , are coupled only via a single spin component  $\gamma = x, y, z$ . As such the edge-sharing 90° bond geometry naturally gives rise to a quantum *compass model* [20], originally introduced by Kugel and Khomskii for the orbital degrees of freedom in Jahn-Teller systems [21] and realized here for the first time in a truly *magnetic* variant. It is precisely this edge-sharing exchange coupling, which has been envisioned [9] to lead to a realization of Kitaev couplings in the honeycomb iridates  $\text{Na}_2\text{IrO}_3$ ,  $\alpha\text{-Li}_2\text{IrO}_3$ , and  $\alpha\text{-RuCl}_3$  and which has later also been found to be realized in the 3D hyper-honeycomb and strip-honeycomb materials  $\beta\text{-Li}_2\text{IrO}_3$  and  $\gamma\text{-Li}_2\text{IrO}_3$ . This second scenario of edge-sharing exchange can be further expanded by considering octahedral geometries where neighboring  $\text{IrO}_6$  octahedra do not share an edge, but have two parallel edges as illustrated in the right-most panel of Fig. 3. Following the exact same line of arguments, one also arrives at a destructive interference for the isotropic Heisenberg exchange in this setting and the emergence of a bond-directional exchange. This latter scenario is realized in triangular Kitaev materials such as  $\text{Ba}_3\text{IrTi}_2\text{O}_9$ .

In passing we note that recently also the microscopics of *face-sharing* octahedra [22] has been discussed, which is relevant, for instance, to the quantum magnetism of  $\text{Ba}_5\text{AlIr}_2\text{O}_{11}$  [23].

Going beyond these symmetry-guided microscopic considerations and performing ab initio calculations [24, 25], one finds that the generic Hamiltonian describing the interactions between  $j = 1/2$  spin-orbit entangled moments of spin-orbit assisted Mott insulators takes the general form

$$H = - \sum_{\gamma\text{-bonds}} J \mathbf{S}_i \mathbf{S}_j + K S_i^\gamma S_j^\gamma + \Gamma \left( S_i^\alpha S_j^\beta + S_i^\beta S_j^\alpha \right), \quad (2)$$

where the sum runs over nearest-neighbor spins at sites coupled by a bond  $\langle i, j \rangle$  along the  $\gamma = (x, y, z)$  direction. The strength of the isotropic Heisenberg coupling is given by  $J$ , and the bond-directional couplings include (i) a Kitaev term of strength  $K$  that couples the component  $\gamma$  of the spins along a  $\gamma$ -bond and (ii) a symmetric off-diagonal exchange  $\Gamma$  that couples the two orthogonal spin components  $\alpha, \beta \perp \gamma$  for a bond along the  $\gamma = x, y, z$  direction. The relative strength and coupling sign of the various couplings varies from material to material, but a common thread in all Kitaev materials is that the Kitaev coupling is the dominant exchange coupling, i.e.  $K > J, \Gamma$ , with a similar ratio of the Kitaev to Heisenberg exchange of  $|K/J| \approx 4$  for many  $j = 1/2$  Mott insulators (for a more detailed discussion, see below). The microscopic model (2), which is also referred to as the  $J\Gamma$  model, is often simplified to the Heisenberg-Kitaev model ( $\Gamma = 0$ ), which has first been conceptualized and studied in the context of the

honeycomb iridates by Chaloupka, Jackeli, and Khaliullin [26]. We will return to this model after a discussion of the pure Kitaev model ( $J, \Gamma = 0$ ) in the next section.

The effect of bond-directional interactions is a strong **exchange frustration** arising from the simple fact that these interactions cannot be simultaneously minimized, as illustrated for Kitaev-type couplings in Fig. 4. Like geometric frustration, its more widely known counterpart that arises when the lattice geometry gives rise to constraints that cannot be simultaneously satisfied, the effect of exchange frustration is to inhibit magnetic ordering and give rise to a residual ground-state entropy. This is true already on the *classical* level. For instance, the classical Kitaev honeycomb model does not exhibit a finite-temperature phase transition [27, 28], but undergoes a thermal crossover to an extensively degenerate Coulomb phase [29] at zero temperature.

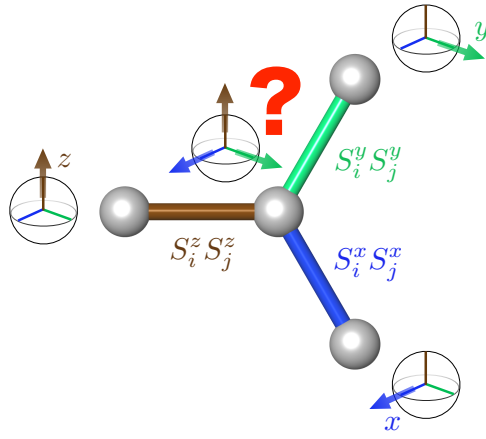


**Fig. 4:** Exchange frustration arising from spin-orbit induced bond-directional interactions, i.e. Ising-like couplings where the exchange easy axis depends on the spatial orientation of an exchange bond. Spins subject to these bond-directional interactions cannot simultaneously minimize all couplings, which holds both for quantum and classical moments.

## 1.2 Kitaev model

The pure Kitaev model, which couples SU(2) spin-1/2 degrees of freedom with bond-directional interactions – Ising-like couplings with a magnetic easy axis sensitive to the spatial orientation  $\gamma$  of the bond (see Figs. 4 and 5 for an illustration)

$$H_{\text{Kitaev}} = - \sum_{\gamma-\text{bonds}} K_\gamma S_i^\gamma S_j^\gamma, \quad (3)$$

is of central interest in condensed matter physics (and beyond). For one, it is famously known for harboring both gapped and gapless quantum spin-liquid ground states. At the same time, it is one of the rare microscopic models that can be solved exactly, as demonstrated in seminal work [19] by Alexei Kitaev in 2006. This analytical tractability allows one to precisely describe and track the fractionalization of the original spin-orbit entangled degrees of freedom  $S_i$  into a fermionic degree of freedom, a so-called Majorana fermion, and a  $Z_2$  gauge field as illustrated in Fig. 5. The  $Z_2$  gauge field turns out to be static, it orders at zero temperature and its elementary vison excitations are found to be massive. The Majorana fermions, on the other hand,

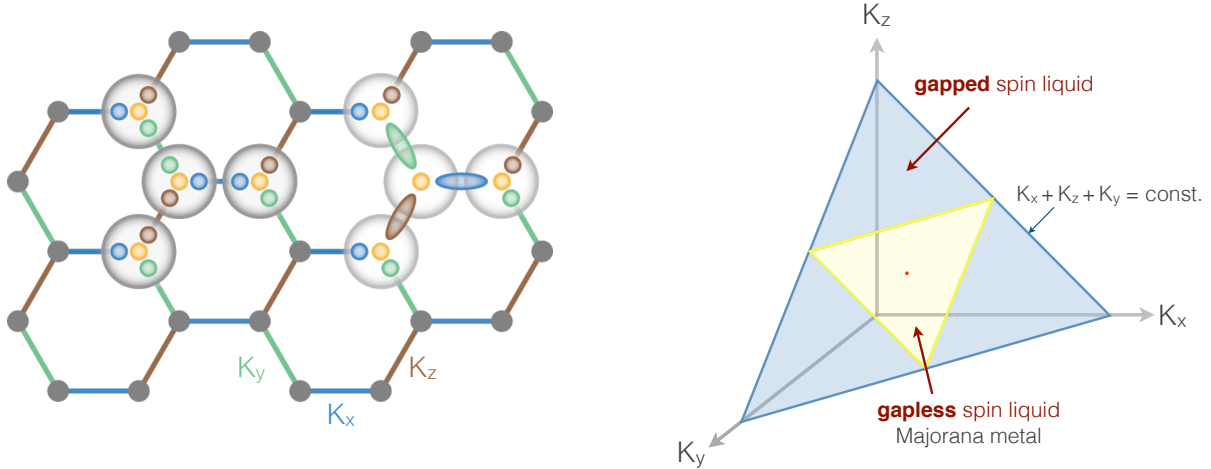


**Fig. 5:** Left: The honeycomb Kitaev model with bond-directional couplings  $K_x$ ,  $K_y$  and  $K_z$ . The model can be analytically solved by introducing four flavors of Majorana fermions (indicated by the yellow, blue, green and brown circles) and recombining them into a static  $Z_2$  gauge field (indicated by the blue, green and brown ovals) and a remaining itinerant Majorana fermion (yellow circle). Right: Phase diagram of the Kitaev model plotted for a plane  $K_x + K_y + K_z = \text{const.}$  If one of the three couplings dominates, the system forms a gapped spin liquid indicated by the blue shading. Around the point of isotropic coupling strengths  $K_x = K_y = K_z$  (indicated by the red dot) a gapless spin liquid emerges, which can be best characterized as a (semi-)metal of the Majorana fermions.

remain itinerant and form a gapless state – a *Majorana metal* – around the point of equal coupling  $K_x = K_y = K_z$ . For the honeycomb lattice, this Majorana metal is a semi-metal with a Dirac cone dispersion (well known from the analogous calculation of free complex fermions for graphene-like electron systems). If one of the three couplings dominates, the system undergoes a phase transition (e.g. for dominant  $K_z$  coupling along the line  $K_z = K_x + K_y$ ) into a gapped spin liquid. This latter state exhibits Abelian ( $Z_2$ ) topological order akin to the well-known toric code model [30] and macroscopic entanglement. Applying a magnetic field along the 111-direction, i.e. coupling the magnetic field to all three spin components, gaps out the gapless spin liquid into an even more exotic spin liquid with non-Abelian (Ising-type) topological order [19]. The non-Abelian character of the latter is identical to that of a  $p_x + ip_y$  superconductor [31], the Moore-Read state [32] proposed for the  $\nu = 5/2$  fractional quantum Hall state, heterostructures of superconductors and topological band insulators [33] or semiconductors [34], as well as that of a network [35] of Majorana wires [36, 37] – all physical systems, which have gathered considerable interest in the context of proposals for fault-tolerant topological quantum computation [30, 38]. Despite this similarity, the search for Kitaev materials and a solid-state realization of the Kitaev model is probably less driven by a potential application in quantum computing technologies, but deeply inspired by the fundamental pursuit of (i) the synthesis of spin liquid materials, (ii) the experimental discovery of Majorana fermions, and (iii) a direct experimental probe of the underlying ( $Z_2$ ) gauge physics – such experimental evidence for gauge physics in a condensed-matter context has long been lacking, despite theorists using the concept of  $Z_2$  gauge theories in the classical statistical mechanics of nematics [39] and to capture the physics of fractionalization in quantum many-body systems [40, 41, 42] for decades.

The conceptual understanding of the physics of the Kitaev model has been steadily growing since its initial description and analytical solution [19]. This includes the fundamental role of vacancies [43, 44], depletion [45], and impurities [46], disorder effects [43, 47, 48], and more exotic phenomena such as the strain-induced formation of Landau levels [49] or topological liquid nucleation [50, 51] arising from vortex-vortex interactions in the non-Abelian phase [52]. The emergence of  $p$ -wave superconductivity upon doping has been discussed [53, 54, 55, 56]. With an eye towards a material realization of the (pure) Kitaev model several experimental signatures have been discussed including the dynamical response [57, 58], whose distinct spectral gap can be probed via inelastic neutron scattering (INS) or electron spin resonance (ESR), the Raman response [59, 60], the inelastic light scattering response [61], which can be probed via resonant Raman scattering, as well as the resonant inelastic X-ray scattering (RIXS) response [62].

Going beyond the pure Kitaev model, considerable attention has been devoted to the Heisenberg-Kitaev model. Its principal phase diagram [63] is shown in Fig. 6 for a parametrization of the coupling strength  $J = \cos \phi$ ,  $K = \sin \phi$ . Besides extended spin liquid phases around the pure Kitaev limit (with either ferro- or antiferromagnetic coupling) there are four magnetically ordered phases. This includes conventional ferromagnetic and Néel ordering around the pure Heisenberg limits, as well as a stripy and a zig-zag ordered phases. The origin of the latter can be readily understood by a duality [7] (sometimes referred to as Klein duality [64]) of these phases to the two conventionally ordered ones. In particular, the Klein duality allows to map the left- and right-hand sides of the circular phase diagram of Fig. 6 onto one another by the relation

$$J \rightarrow -J \quad \text{and} \quad K \rightarrow 2J + K, \quad (4)$$

and a concurrent four-sublattice rotation [7]. This duality thereby connects the ferromagnet to the stripy phase, and the Néel ordered state to the zig-zag ordered phase (as well as the spin liquid phases onto themselves).

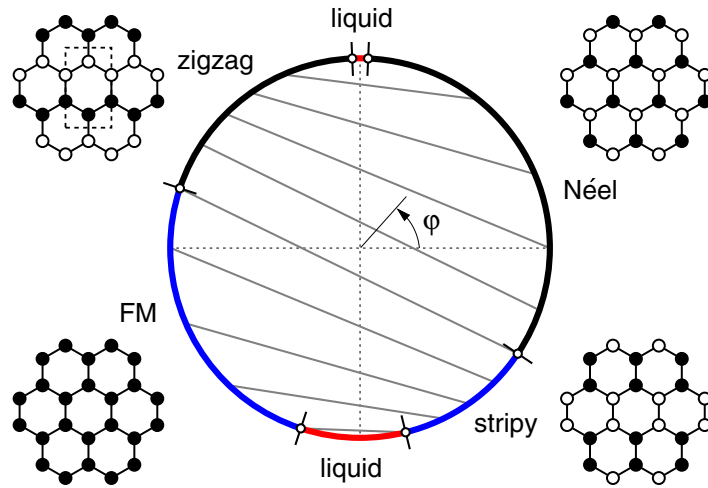


**Fig. 6:** Phase diagram of the Heisenberg-Kitaev model, reproduced from Ref. [63].

The conceptual understanding of this extended model has been furthered by a discussion of its finite-temperature physics [65] and dynamical response [66] along with the effects of an applied magnetic field [67], lattice distortions [28], as well as the inclusion of further neighbor Heisenberg [68] and Kitaev [69] interactions. The potentially multicritical point at the phase

transition between the spin liquid and the magnetically ordered phases has been investigated both numerically [67] and analytically [70]. The dynamical spin structure factor beyond the Kitaev limit has recently been discussed [71] as have been liquid-liquid transitions upon introducing an additional Ising coupling [72]. Extensions including charge fluctuations have also been discussed [73]. Finally, a classical variant of the Heisenberg-Kitaev model has also been explored [74, 75, 28], including the formation of spin textures in a magnetic field [76, 77].

## 2 Honeycomb Kitaev materials

The quest to synthesize and explore Kitaev materials has been kick-started in 2009 by the profound theoretical vision of Jackeli and Khaliullin [9] that laid out in remarkably precise terms what the elementary ingredients (in its literal sense) for a successful material search strategy are. In particular, they not only explained the microscopic origin of Kitaev-type bond-directional exchange interactions in certain (edge sharing)  $4d^5$  and  $5d^5$  transition metal compounds (as reviewed in the previous section). They also laid out a detailed proposal for a material realization of the honeycomb Kitaev model in the iridate  $\alpha\text{-Li}_2\text{IrO}_3$  and, more generally, iridates of the form  $A_2\text{IrO}_3$  with a crystal structure as illustrated in Fig. 7 – a proposal that was quickly refined [26] to also include  $\text{Na}_2\text{IrO}_3$  which, at the time, had already been synthesized [78, 79] and scrutinized as a potential topological insulator [80].

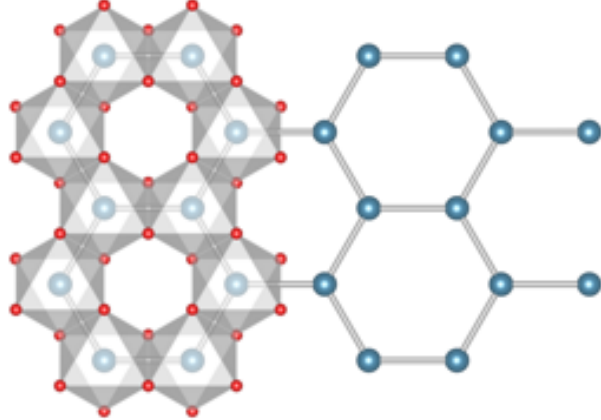


**Fig. 7:** Crystal structure of the honeycomb Kitaev materials  $A_2\text{IrO}_3$  such as  $\text{Na}_2\text{IrO}_3$  and  $\alpha\text{-Li}_2\text{IrO}_3$ .

### 2.1 $\text{Na}_2\text{IrO}_3$

$\text{Na}_2\text{IrO}_3$  was independently synthesized to explore its potential for Kitaev physics in 2009/2010 by the groups of Takagi [78] and Gegenwart [79]. Since then samples have been grown in a number of labs around the world, including large single-crystals of diameters up to 10 mm in the group of Cao [81]. With samples readily available, numerous experimental probes have been taken that have revealed that  $\text{Na}_2\text{IrO}_3$  is indeed a Mott insulator with an insulating gap of  $\Delta = 340$  meV (opening at around 300 K) measured in optical transmission experiments [82]. Fits of the magnetic susceptibility confirm the predominant  $j = 1/2$  nature of the local moments indicating magnetic moments of  $1.79(2)\mu_B$  [79, 83], rather close to the value of  $1.74\mu_B$  expected for spin 1/2 moments, while X-ray absorption spectroscopy [84] points to a

small admixture of  $j = 1/2$  and  $j = 3/2$  states. Resonant inelastic x-ray scattering (RIXS) [85, 86] finds evidence for a small trigonal distortion of the  $\text{IrO}_6$  octahedra resulting in a crystal field splitting of the  $j = 3/2$  states of about 110 meV, which, however, is considerably smaller than the typical strength of the spin-orbit coupling of the iridates  $\lambda \approx 400 - 500$  meV [87, 88]. The system, however, does not exhibit the sought after spin liquid ground state, but is found to magnetically order at around  $T_N = 15$  K, a temperature significantly below the Curie-Weiss temperature of  $\Theta_{\text{CW}} = -125$  K [83]. The suppression of the ordering temperature with regard to the Curie-Weiss temperature indicates magnetic frustration which, quantified by the ratio  $f = |\Theta_{\text{CW}}|/T_N \approx 8$ , is unusually high for a quantum magnet on a bipartite lattice. It has been rationalized [65, 83] to arise from geometric frustration arising from next-nearest neighbor couplings within the elementary hexagons of the honeycomb structure and is not indicative of a close proximity to the Kitaev spin liquid. The exact form of the magnetic ordering was subsequently determined to be of zig-zag type by resonant x-ray magnetic scattering [89] and inelastic neutron scattering [81, 90]. The microscopic origin of this zig-zag ordering has been scrutinized in light of the Heisenberg-Kitaev model [63] supplemented with next-nearest neighbor Heisenberg [83] and Kitaev [91, 92] couplings along with a flurry of ab initio calculations [93, 94, 95, 84] and, most recently, dynamical mean-field studies [96].

Probably the best experimental evidence that  $\text{Na}_2\text{IrO}_3$  should indeed be considered to be the first Kitaev material to be synthesized comes from diffuse magnetic X-ray scattering [97], which has provided a direct experimental observation of bond-directional exchange and a dominant Kitaev coupling.

Several ideas have been put forward to bring  $\text{Na}_2\text{IrO}_3$  closer to the Kitaev spin liquid regime, such as the making of thin films [98] or heterostructures [99], but probably the most practical scheme has been to replace the Na atoms by the smaller Li atoms and instead explore the physics of  $\text{Li}_2\text{IrO}_3$ .

## 2.2 $\alpha$ - $\text{Li}_2\text{IrO}_3$

The exploration of  $\text{Li}_2\text{IrO}_3$  as candidate Kitaev material has indeed lent further impetus to the field. Probably the biggest surprise came when its synthesis lead to the discovery of several polymorphs [83, 100, 101] which have been dubbed  $\alpha$ - $\text{Li}_2\text{IrO}_3$ ,  $\beta$ - $\text{Li}_2\text{IrO}_3$ , and  $\gamma$ - $\text{Li}_2\text{IrO}_3$  in the sequence of their discovery. Only  $\alpha$ - $\text{Li}_2\text{IrO}_3$  is isostructural to  $\text{Na}_2\text{IrO}_3$  and exhibits iridium honeycomb layers (as depicted in Fig. 7), while the other two polymorphs,  $\beta$ - $\text{Li}_2\text{IrO}_3$  and  $\gamma$ - $\text{Li}_2\text{IrO}_3$ , have been found to exhibit three-dimensional, tricoordinated networks of the iridium ions. We will discuss the latter in the context of three-dimensional Kitaev materials below.

The first high-quality samples of  $\alpha$ - $\text{Li}_2\text{IrO}_3$  have been synthesized by the Gegenwart group [83] in 2012. Magnetic susceptibility fits reveal magnetic moment of  $1.83(5)\mu_B$ , a value slightly larger than expected for spin-1/2 degrees of freedom [83]. Like its sister compound  $\text{Na}_2\text{IrO}_3$ ,  $\alpha$ - $\text{Li}_2\text{IrO}_3$  undergoes a magnetic ordering transition at  $T_N = 15$  K with a Curie-Weiss temperature of  $\Theta = -33$  K. Thin films of  $\text{Li}_2\text{IrO}_3$  created by pulsed laser deposition on  $\text{ZrO}_2:\text{Y}$  (001) single crystalline substrates reveal [102] a small optical gap of 300 meV indicative of a Mott gap of similar size as in its sister compound  $\text{Na}_2\text{IrO}_3$ .

The further experimental analysis of  $\alpha$ - $\text{Li}_2\text{IrO}_3$  has been largely hampered by the fact that (in contrast to  $\text{Na}_2\text{IrO}_3$ ) it has remained extremely challenging to synthesize bulk single-crystals – an essential ingredient e.g. for neutron scattering studies, in particular to compensate for the large neutron absorption cross-section of the iridium ions. The early powder samples were found to exhibit single-crystalline ordering only on length scales smaller than 10  $\mu\text{m}$ . Re-

cent experimental progress, however, has pushed this boundary to about a millimeter [103]. These single crystals have been sufficiently large to allow resonant magnetic x-ray diffraction combined with powder magnetic neutron diffraction to reveal an incommensurate magnetic ordering where the magnetic moments in iridium honeycomb layers are *counter-rotating* on nearest-neighbor sites [104]. Prior to its experimental observation a number of theoretical proposals [24, 105, 106, 107] for spiral or other forms of incommensurate magnetic ordering in this honeycomb material have been put forward, none of which envisioned counter-rotating spirals. However, a very similar magnetic ordering is observed in the three-dimensional  $\beta\text{-Li}_2\text{IrO}_3$  and  $\gamma\text{-Li}_2\text{IrO}_3$  polymorphs where subsequent theoretical analysis has lead to a unifying theory [108, 109] of counter-rotating spiral magnetism in all three compounds. The minimal model to explain the occurrence of counter-rotating spirals appears to be a Kitaev model supplemented with small Heisenberg and Ising interactions [104] with theoretical estimates indicating that the Kitaev interaction might be up to a factor of 20 larger than the Heisenberg exchange [108].

Taking a step back,  $\alpha\text{-Li}_2\text{IrO}_3$  remains much less explored than its sister compound  $\text{Na}_2\text{IrO}_3$  despite its somewhat more unconventional magnetism, whose origin in a vastly enhanced Kitaev coupling puts  $\alpha\text{-Li}_2\text{IrO}_3$  probably much closer to the sought-after Kitaev spin liquid than  $\text{Na}_2\text{IrO}_3$ . This leads to the tempting observation that replacing the Na atoms by Li atoms indeed pushed the system closer to the Kitaev regime and that the next logical step would be to replace Li by an even smaller atom, i.e. hydrogen. While a small step for a theorist to contemplate, this amounts to a big leap for material synthesis. But it is precisely this leap, which the Takagi group seems to have taken in the last few months by successfully synthesizing  $\alpha\text{-H}_{3/4}\text{Li}_{1/4}\text{IrO}_3$  – a hydrogen intercalated layered honeycomb iridate that shows a Curie-Weiss behavior consistent with a  $j = 1/2$  Mott insulator, no evidence of magnetic ordering, and no NMR line broadening down to the lowest temperatures [110]. These are prime indicators that this material might indeed realize a Kitaev spin liquid.

### 2.3 $\alpha\text{-RuCl}_3$

In parallel, another material has taken center stage in the search for Kitaev materials – the 4d compound  $\alpha\text{-RuCl}_3$ . The material consists of very weakly bounded layers of edge-sharing  $\text{RuCl}_6$  octahedra (of almost perfect cubic symmetry with no trigonal distortions) with the central  $\text{Ru}^{3+}$  ( $4d^5$ ) ions forming an almost ideal honeycomb lattice. Originally thought to be a conventional semiconductor in early 1970's transport measurements [111], spectroscopic measurements in the mid 1990's pointed towards the formation of a Mott insulator [112]. It was only in 2014 that the group of Young-June Kim realized that  $\alpha\text{-RuCl}_3$  is in fact a spin-orbit assisted  $j = 1/2$  Mott insulator [113]. Direct evidence for Mott physics in  $\alpha\text{-RuCl}_3$  comes from optical spectroscopy [113] measuring an optical gap of 200 meV and angle-resolved photoemission spectroscopy (ARPES) [114] observing a charge gap of 1.2 eV at temperatures of 200 K. The strength of the spin-orbit coupling has been determined from optical spectroscopy [115] to be  $\lambda \approx 100$  meV and from neutron scattering experiments on polycrystalline samples [116] to be  $\lambda \approx 130$  meV, both estimates somewhat smaller than the atomic spin-orbit coupling  $\lambda \approx 150$  meV for ruthenium [117]. While the strength of the spin-orbit coupling in this 4d compound is thus considerably smaller than for the heavier 5d iridates, it has been argued on the basis of ab initio calculations [113] that the *ratio* of the spin-orbit coupling and the electronic bandwidth is only slightly smaller than in the iridates and still suffices to induce the formation of spin-orbit entangled  $j = 1/2$  and  $j = 3/2$  bands. The formation of  $j = 1/2$  local moments is further supported by Curie-Weiss fits [118, 119] of the magnetic susceptibility

yielding a magnetic moment of  $2.2\mu_B$  (somewhat above the expected value of  $1.74\mu_B$  for a spin-1/2) and by angle-resolved photoemission, x-ray photoemission, and electron energy loss spectroscopy [120, 121]. Scanning transmission electron and scanning tunneling microscopies [122] on exfoliated/cleaved  $\alpha$ -RuCl<sub>3</sub> samples report a Mott gap of 250 meV in the measured density of states, slightly larger than the value obtained for bulk samples in optical spectroscopy, and a subtle charge ordering pattern originating from anisotropy in the charge distribution along Ru-Cl-Ru hopping pathways.

In exploring the magnetism of  $\alpha$ -RuCl<sub>3</sub>, susceptibility measurements on powder samples [118, 119] indicate a Curie-Weiss temperature of around 23 – 40 K consistent with single-crystal measurements [123] of the in-plane susceptibility yielding a value of  $\Theta_{CW} = 37$  K, while the out-of-plane susceptibility reveals a value of  $\Theta_{CW} = -150$  K. At first two successive ordering transitions at 7 K and 15 K have been reported, both in specific heat and susceptibility measurements on powder samples [123] as well as in single-crystal inelastic neutron scattering experiments [116], with the higher transition later attributed to the presence of stacking faults in less pristine samples of  $\alpha$ -RuCl<sub>3</sub> and entirely absent in high-quality single-crystals probed by X-ray diffraction [124] and inelastic neutron scattering [125] experiments. Below  $T_N = 7$  K pristine  $\alpha$ -RuCl<sub>3</sub> exhibits zig-zag magnetic ordering (similar to that of Na<sub>2</sub>IrO<sub>3</sub>) confirmed in various experimental probes including neutron [126, 127] and X-ray [128, 124] diffraction experiments, inelastic neutron scattering on polycrystalline [116] and single-crystal [125] samples along with muon spin rotation measurements [129]. The emergence of zig-zag magnetic ordering in  $\alpha$ -RuCl<sub>3</sub> is also consistent with ab initio calculations [130, 128, 131, 132] and microscopic calculations for the HKT model (2) [92] and variations thereof [133]. The strength of the Kitaev coupling in  $\alpha$ -RuCl<sub>3</sub> has been estimated to be of the order of 100 K in thermal conductivity measurements [134].

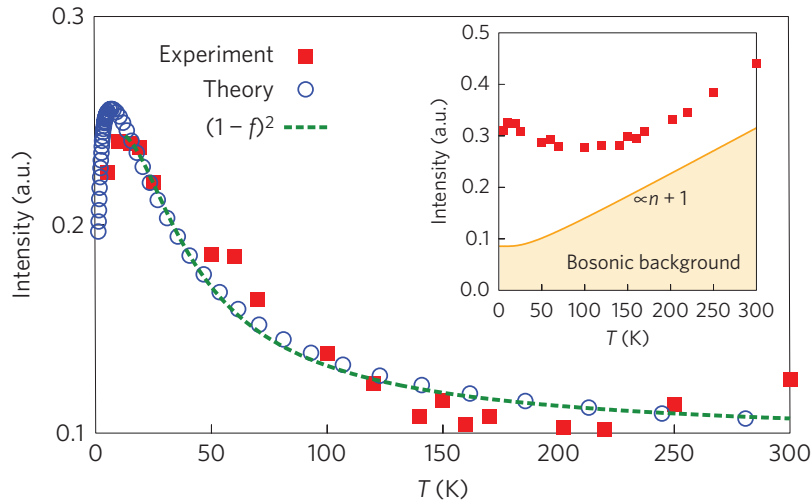


**Fig. 8:** Interpretation of the Raman scattering data of  $\alpha$ -RuCl<sub>3</sub>. The inset shows the raw experimental Raman scattering intensities [135], from which a (phononic) background contribution (indicated by the shaded area) is subtracted. The remaining contribution is shown in the main panel and compared to  $(1 - f)^2$ , i.e. the asymptotic two-fermion-scattering form where  $f$  is the Fermi distribution function, and numerical results [136] from quantum Monte Carlo simulations (squares). Figure reproduced from Ref. [136].

What sets  $\alpha$ -RuCl<sub>3</sub> apart from the honeycomb iridates Na<sub>2</sub>IrO<sub>3</sub> and  $\alpha$ -Li<sub>2</sub>IrO<sub>3</sub> is that several unusual features *above* the magnetic ordering transition can be interpreted as arising from a close proximity to a Kitaev spin liquid. Here we want to highlight three such features found in Raman scattering and inelastic neutron scattering experiments of  $\alpha$ -RuCl<sub>3</sub>.

We start with the Raman scattering experiments performed by Sandilands and collaborators [135, 115]. Upon close inspection of the original Raman data [135] plotted in the inset of Fig. 8, it has been argued by Nasu *et al.* [136] that the experimental data exhibits direct evidence of *fermionic* excitations across a broad energy and temperature range. This is an extraordinary observation, since the excitations of ordinary magnetic insulators, magnons and phonons, obey bosonic statistics. In the context of Kitaev spin liquids, however, fermionic excitations arise naturally, as one of the defining aspects of these spin liquids is the fractionalization of the original spin degrees of freedom into a Z<sub>2</sub> gauge field and a Majorana *fermion*. This should also hold for systems in close proximity to such a Kitaev spin liquid, which is precisely what Nasu *et al.* argue is the case for  $\alpha$ -RuCl<sub>3</sub> [136]. The experimental evidence that is considered in their argument is the temperature dependence of the measured Raman intensity – after subtraction of what is identified as a (bosonic) background contribution, which is attributed to phonons as it persists up to very high temperatures much larger than any magnetic scale. The remaining intensity distribution, plotted in the main panel of Fig. 8, is found to be very well approximated by  $(1 - f)^2$ , i.e. the asymptotic two-fermion scattering form where  $f$  is the Fermi distribution function. An almost perfect fit is obtained when calculating the Raman intensity via quantum Monte Carlo techniques [137]. This is an intriguing result – taken at face value, it is the first experimental indication for the emergence of (Majorana) fermion excitations in a bulk magnetic insulator. However, it should be noted that the interpretation of the experimental Raman data **hinges** – in a crucial manner – on the specific way that the (phononic) background contribution is identified and subtracted, an often subtle and not completely unambiguous procedure.

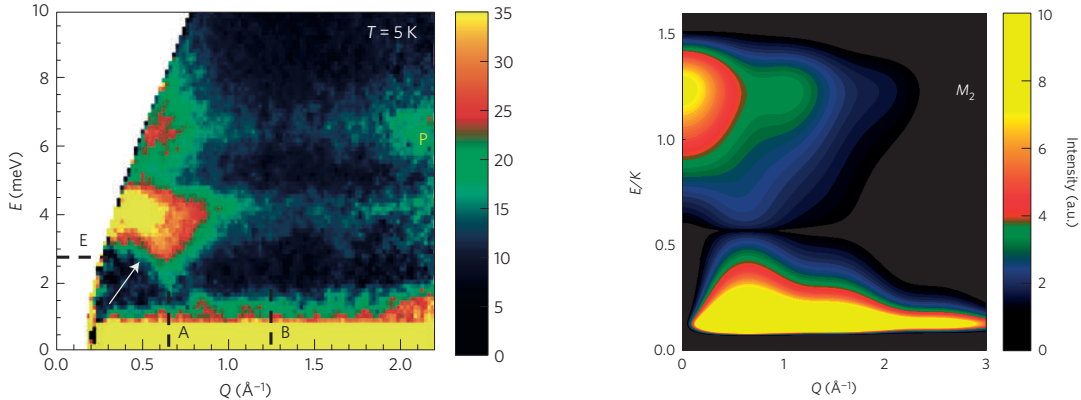


**Fig. 9:** Left: False color plot of the inelastic neutron scattering data of  $\alpha$ -RuCl<sub>3</sub>. Two magnetic modes with band centers around  $E = 4$  and  $6$  meV are identified. While the lower one is attributed to the concave spin wave dispersion on a zig-zag ordered background (indicated by the white arrow), the upper feature resembles the broad, non-dispersive high-energy response expected of a Kitaev spin liquid. Right: Analytical calculation of the dynamical response of the Kitaev spin liquid. Above a low-energy band a broad feature is found that is strongest at  $Q = 0$  and decreases with increasing  $Q$ . Figures reproduced from Ref. [116].

Two more experimental features strongly support the idea that  $\alpha$ -RuCl<sub>3</sub> is indeed in close proximity to a Kitaev spin liquid, both of them are found in the magnetic scattering observed in inelastic neutron scattering experiments [116, 125]. While at low energies the scattering is consistent with spin waves on a zig-zag ordered background, a broad scattering continuum is found at higher energies. It is this second magnetic mode that resembles the broad, non-dispersive high-energy response expected of a Kitaev spin liquid [116]. A comparison of the experimental neutron scattering data with exact analytical calculations of the dynamical response of the Kitaev model are given in Fig. 9. At intermediate energy scales there are star-like features (reproduced in Fig. 10 [125]), which arise from the interplay of spin wave and spin liquid physics in this regime. While the dynamical response of the pure Kitaev model does not show this star-like feature, it can be explained by the small admixture of additional neighbor correlations as induced, for instance, by the inclusion of a Heisenberg exchange and experimentally observed in optical spectroscopy [138]. Indeed, recent numerical studies [66] of the dynamical response of the Heisenberg-Kitaev model have quantitatively reproduced the star-like feature.

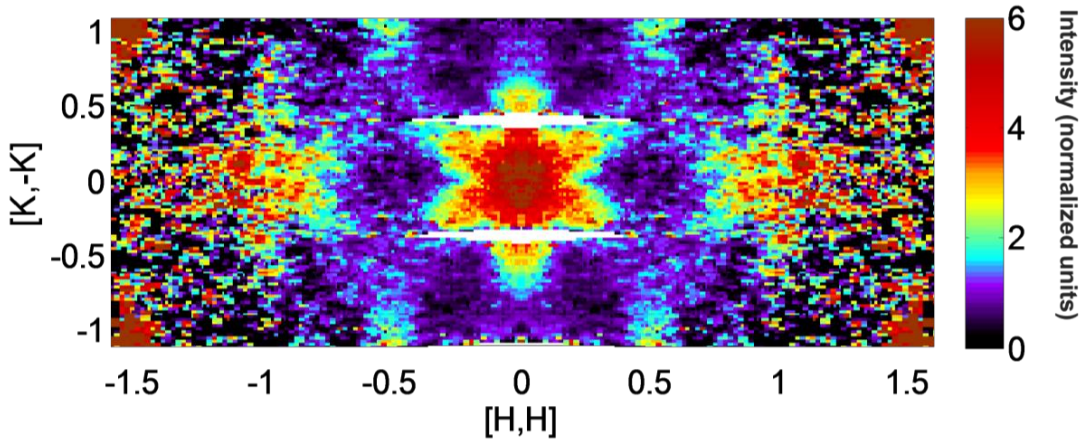


**Fig. 10:** Extended zone picture of neutron scattering data of  $\alpha$ -RuCl<sub>3</sub> integrated over the energy window [4.5, 7.5] meV and symmetrized along the  $(H, H, 0)$ -direction taken at  $T = 10$  K, i.e. well above the magnetic ordering transition at  $T_N = 7$  K. The star-like feature at the zone center arises from the interplay of spin wave and spin liquid physics in this temperature regime and can be rationalized within the context of the Heisenberg-Kitaev model [66]. Figure reproduced from Ref. [125].

In total, the mounting experimental data on  $\alpha$ -RuCl<sub>3</sub> support the proposal that, although  $\alpha$ -RuCl<sub>3</sub> magnetically orders, it is in such close proximity to a Kitaev spin liquid that remnants of decisive spin-liquid features can still be probed *above* the magnetic ordering transition. This includes experimental evidence for fermionic quasiparticles in Raman scattering [135, 136], a broad magnetic continuum in inelastic neutron scattering [116] and the star-like feature [125, 66] above the magnetic ordering transition in inelastic neutron scattering.

Let us finally mention that also  $\alpha$ -RuCl<sub>3</sub> has a polymorph,  $\beta$ -RuCl<sub>3</sub>, in which face-sharing RuCl<sub>6</sub> octahedra are arranged in chains.  $\beta$ -RuCl<sub>3</sub> is found to show no magnetic ordering down to 5 K [118] and awaits further experimental analysis.

### 3 Triangular Kitaev materials

Beyond the search for spin liquids, Kitaev materials also provide ample opportunity to study other unconventional forms of magnetism. A particularly interesting class might be materials in which  $j = 1/2$  moments form quasi-two-dimensional *triangular* lattice structures, such as the family of hexagonal perovskites  $\text{Ba}_3\text{Ir}_x\text{Ti}_{3-x}\text{O}_9$ , in particular the sister compounds  $\text{Ba}_3\text{IrTi}_2\text{O}_9$  ( $x = 1$ ) [139] and  $\text{Ba}_3\text{TiIr}_2\text{O}_9$  ( $x = 2$ ) [140]. It has recently been argued [141] that the microscopic description of the former is captured by a triangular Heisenberg-Kitaev model.

The interplay of geometric and exchange frustration in this model leads to the formation of non-trivial spin textures [142, 141], such as the formation of a  $Z_2$ -vortex crystal induced by the Kitaev couplings that destabilize the  $120^\circ$  order of the (antiferromagnetic) quantum Heisenberg model.

#### 3.1 $\text{Ba}_3\text{Ir}_x\text{Ti}_{3-x}\text{O}_9$

The 2012 synthesis of  $\text{Ba}_3\text{IrTi}_2\text{O}_9$  ( $x = 1$ ) by the group of Mahajan [139] marks the discovery of the first triangular  $j = 1/2$  Mott insulator. It is now recognized as the first representative of a family of hexagonal  $j = 1/2$  iridium perovskites of the form  $\text{Ba}_3\text{Ir}_x\text{Ti}_{3-x}\text{O}_9$ , of which various members with  $1 \leq x \leq 2$  have been synthesized over the last years [143]. The crystal structure of these perovskites – which are found to exhibit hexagonal space group symmetries  $P6_3mc$  ( $x = 1$ ) [139] or  $P6_3/mmc$  ( $x = 2$ ) [140], respectively – is illustrated in Fig. 11. Generically, the structure is composed of three layers of  $[\text{Ir}/\text{TiO}_6]$  octahedra, two of which form a double-layer of face-sharing  $\text{Ir}_2\text{O}_9$  biotahedra (indicated by the blue octahedra) and a single layer (indicated by the light brown octahedra). The occupation of the octahedral sites in the different layers with  $\text{Ir}^{4+}$  and  $\text{Ti}^{4+}$  ions is complicated by the fact that the two ions have rather similar radius. For  $\text{Ba}_3\text{Ir}_2\text{TiO}_9$ , it is found that the iridium ions fill all octahedral sites in the double-layer [140], which are then well separated by a single layer of (non-magnetic) titanium ions. For  $\text{Ba}_3\text{IrTi}_2\text{O}_9$  a more complicated picture emerges with the iridium ions still preferably occupying octahedral sites in one of two double-layers, but a significant amount of site inversion ( $7 \pm 4\%$ ) with the titanium ions from the other double-layer has been reported [139].

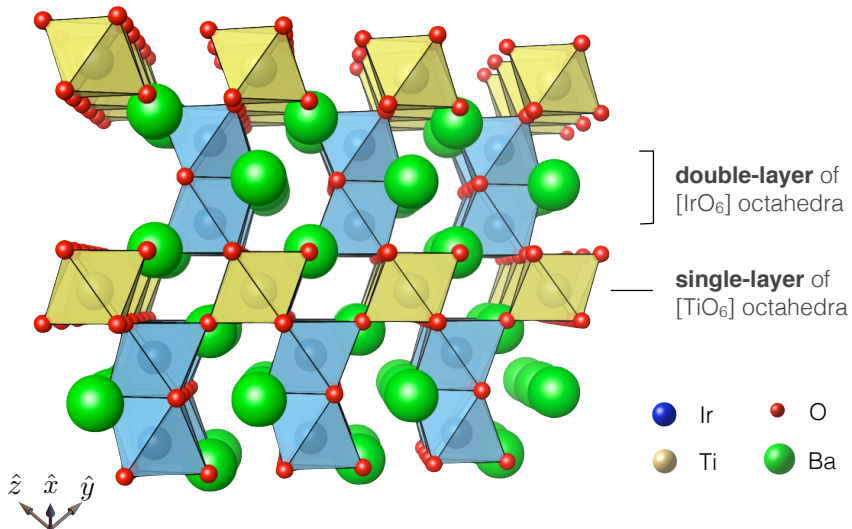


**Fig. 11:** Crystal structure of the triangular Kitaev material  $\text{Ba}_3\text{Ir}_2\text{TiO}_9$  [140].

Magnetic susceptibility and heat capacity data [139] for  $\text{Ba}_3\text{IrTi}_2\text{O}_9$  show no magnetic ordering down to  $0.35\text{ K}$  in spite of a strong antiferromagnetic coupling as evidenced by a large Curie-Weiss temperature  $\Theta_{CW} \sim -130\text{ K}$ . The effective moment is theoretically argued to be a spin-orbit entangled  $j = 1/2$  moment (on the basis of ab initio calculations [144]), despite the considerable suppression of the experimentally determined magnetic moment of  $1.09\mu_B$  [139].

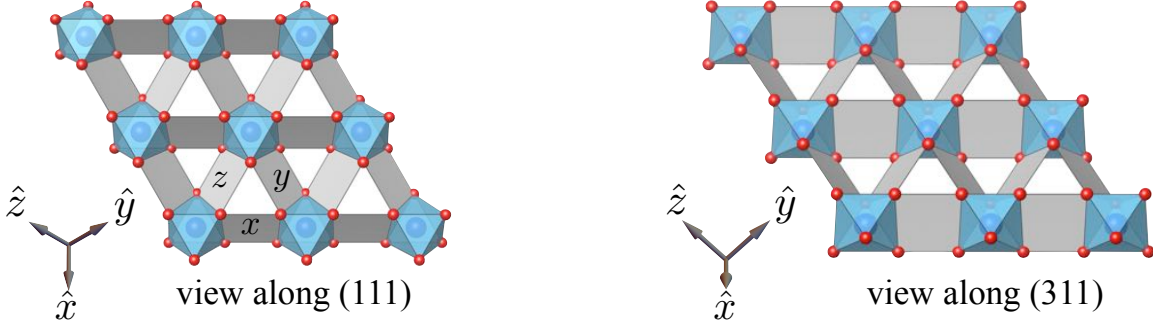


**Fig. 12:** Views of the triangular layer of  $\text{IrO}_6$  octahedra from two different perspectives.

The unconventional magnetism of spin-orbit entangled  $j = 1/2$  moments on a triangular lattice again arises from the presence of bond-directional exchange couplings. On a microscopic level, it has been argued [141] that the arrangement of the  $\text{IrO}_6$  octahedra within the layers, depicted in Fig. 12, fulfills the two necessary ingredients for Kitaev-type interactions. First, neighboring octahedra exhibit parallel edges, which gives rise to two separate exchange paths for every pair of iridium ions. As in the case of edge-sharing  $\text{IrO}_6$  octahedra, this leads to a destructive interference and subsequent suppression of the isotropic Heisenberg exchange [7, 9, 26]. Second, there are three distinct exchange paths for the three principal bond directions of the triangular lattice, with each cutting through *different* edges of the  $\text{IrO}_6$  octahedra. This results in a distinct locking of the exchange easy axis [7, 9, 26] along the three principal lattice directions as illustrated in Fig. 12. Since the Ir layer is normal to the  $111$  direction (see the left panel in Fig. 12), the strength of the bond-directional coupling is equivalent in all three directions. Ultimately, this gives rise to the bond-directional exchange of a triangular Kitaev model. In total, these microscopic considerations lead to a triangular Heisenberg-Kitaev model as the most elementary description for the magnetism in  $\text{Ba}_3\text{IrTi}_2\text{O}_9$ . Ab initio calculations [144] complete this picture by arguing that in addition a symmetric off-diagonal exchange  $\Gamma$  should be considered along with the possible emergence of a Dzyaloshinskii-Moriya (DM) exchange term arising from distortions in the oxygen octahedra, which break inversion symmetry about the Ir-Ir bond center.

The prevalent feature of the magnetism of the triangular Heisenberg-Kitaev model is the emergence of non-trivial spin textures [142, 141]. The Kitaev exchange destabilizes the  $120^\circ$  order of the Heisenberg antiferromagnet and induces a lattice of  $Z_2$ -vortices [142] whose spatial separation is inversely proportional to the strength of the Kitaev coupling (independent of its sign). The resulting phase diagram of the Heisenberg-Kitaev model has been explored both in its classical [142] and quantum [141, 145, 146, 147] variants using a combination of analytical and numerical techniques. A summary is given in Fig. 13.

Finally, we note that other non-trivial spin textures beyond the  $Z_2$ -vortex crystal can be stabilized by spin-orbit coupling effects. For instance, a Dzyaloshinskii-Moriya (DM) exchange also destabilizes the  $120^\circ$  order of the Heisenberg antiferromagnet and instead favors the formation of a skyrmion crystal in the presence of a magnetic field [148, 149].

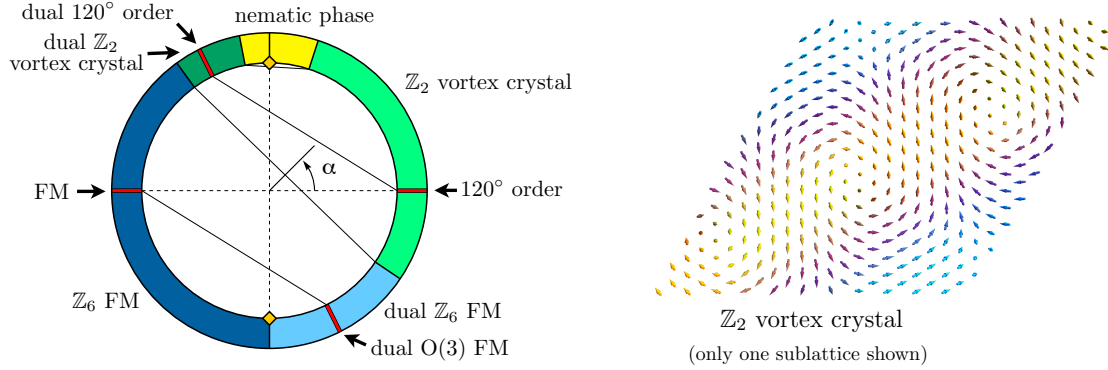


**Fig. 13:** Phase diagram of the triangular Heisenberg-Kitaev model, reproduced from Ref. [141].

Returning to the family of  $\text{Ba}_3\text{Ir}_x\text{Ti}_{3-x}\text{O}_9$  materials, it would be most intriguing to experimentally establish the emergence of non-trivial spin textures in  $\text{Ba}_3\text{IrTi}_2\text{O}_9$ . This, however, requires high-quality single crystals (without the aforementioned Ir/Ti site inversion) that would allow for inelastic neutron scattering experiments. The magnetism of the sister compound  $\text{Ba}_3\text{TiIr}_2\text{O}_9$  is likely dominated by the formation of dimers in the Iridium double-layer and is currently being explored both theoretically and experimentally.

### 3.2 Other materials

Recently, a new family of hexagonal  $j = 1/2$  iridium perovskites of the form  $\text{Ba}_3M\text{Ir}_2\text{O}_9$  with  $M = (\text{Sc}, \text{Y})$  has been experimentally explored [150, 151]. In contrast to the  $\text{Ba}_3\text{Ir}_x\text{Ti}_{3-x}\text{O}_9$  compounds, the (average) iridium valence here is  $\text{Ir}^{4.5+}$ . This possibly leads to a scenario wherein the double-layer one has one effective spin-orbit entangled  $j = 1/2$  moment per face-sharing  $\text{Ir}_2\text{O}_9$  bioctahedra. As argued above, the latter are coupled via three distinct parallel (bi)octahedral edges and as such the effective  $j = 1/2$  moments are likely subject to a bond-directional exchange. While both  $\text{Ba}_3\text{ScIr}_2\text{O}_9$  and  $\text{Ba}_3\text{YIr}_2\text{O}_9$  have been reported to exhibit magnetic ordering at around 10 K (Sc) and 4.5 K (Y), respectively, the closely related  $\text{Ir}^{4.5+}$ -compound  $\text{Ba}_3\text{InIr}_2\text{O}_9$  [140] does not exhibit any sign of magnetic ordering down to 250 mK [152] and, thus, is a potential  $j = 1/2$  spin liquid candidate system.

Another related spin liquid candidate material is the recently synthesized ruthenate  $\text{Ba}_3\text{ZnRu}_2\text{O}_9$  [153], in which a hexagonal lattice of  $\text{Ru}^{5+}$  dimers (with  $S = 3/2$ ) forms in the double-layer of face-sharing  $\text{Ru}_2\text{O}_9$  bioctahedra. The absence of long-range magnetic order down to 37 mK along with a linear specific heat [153] indicate the possible formation of a spin liquid in this material, which would be remarkable given the rather large effective magnetic moment of  $S = 3/2$ .

## 4 Three-dimensional Kitaev materials

The exploration of three-dimensional Kitaev materials was kick-started with the independent, but almost concurrent synthesis of two  $\text{Li}_2\text{IrO}_3$  polymorphs in 2013 –  $\beta$ - $\text{Li}_2\text{IrO}_3$  in Takagi's group [100] and  $\gamma$ - $\text{Li}_2\text{IrO}_3$  in the group of Analytis [101]. Both polymorphs realize truly three-dimensional, but still tricoordinated sublattices of the iridium  $5d^5$  ions, dubbed the hyper-honeycomb and stripy-honeycomb, respectively. As such, these compounds are candidate materials for the realization of three-dimensional Kitaev physics, which we will briefly review in the following before returning to the materials.

## 4.1 Conceptual overview

On a conceptual level, it has been realized early on that the original honeycomb Kitaev model [19] can be generalized to other lattice structures and retain its analytical tractability if one preserves one essential feature of the honeycomb lattice – the *tricoordination* of its vertices. This idea has been exploited, for instance, by Yao and Kivelson [154] in designing a decorated honeycomb lattice for which the Kitaev model exhibits a *chiral spin liquid* – a distinct gapped spin liquid originally proposed by Kalmeyer and Laughlin in 1987 [155] as a bosonic analog of the fractional quantum Hall effect<sup>1</sup>. The potential for *three-dimensional* generalizations of the Kitaev model<sup>2</sup> has first been explored by Mandal and Surendran [163] by considering a site-depleted cubic lattice, a tricoordinated lattice structure which turns out to be isomorphic to the hyper-honeycomb lattice later identified in the context of the iridium sublattice in  $\beta\text{-Li}_2\text{IrO}_3$ . This first three-dimensional generalization of a Kitaev model illustrates that much of the physics of the two-dimensional honeycomb Kitaev models carries over to higher dimensions: The original spin degrees of freedom again fractionalize into Majorana fermions coupled to a  $Z_2$  gauge field. As in the two-dimensional case, the gauge field remains static, which again allows to analytically track the model by (i) solving a basically classical problem identifying the ground state of the  $Z_2$  gauge field and (ii) subsequently diagonalizing a free fermion Hamiltonian describing the physics of the remaining itinerant Majorana fermions (coupled to a fixed gauge field configuration). The result is a gapless spin liquid whose nodal structure is no longer a pair of Dirac cones (as for the two-dimensional honeycomb model), but in fact a *line* of Dirac cones [163]. This result has foreshadowed a more systematic understanding of three-dimensional Kitaev models [164] obtained from a systematic classification of the gapless spin liquids in Kitaev models on the most elementary tricoordinated lattices in three spatial dimensions.

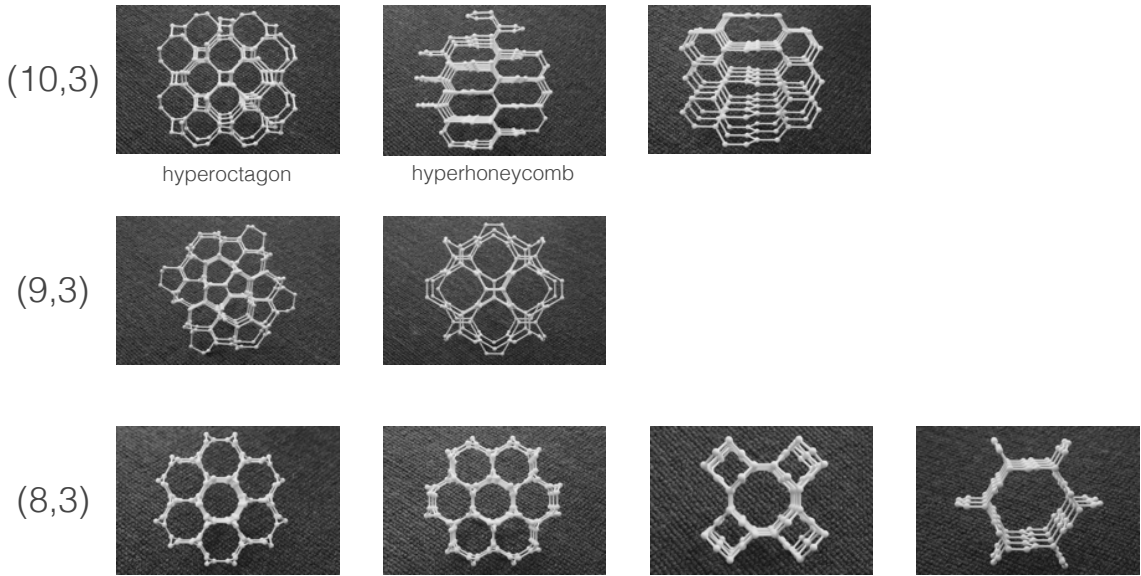


**Fig. 14:** Illustration of the elementary tricoordinated lattices by photographs of 3D printed models. Further information on these lattices is provided in Table 1.

<sup>1</sup>Microscopic realizations of this long sought-after spin liquid in  $SU(2)$  invariant quantum magnets have more recently been established in certain kagome systems [156, 157, 158, 159].

<sup>2</sup> Alternative approaches to generalize the Kitaev model to three spatial dimensions also include higher spin generalizations such as a spin-3/2 Kitaev-type model on the diamond lattice [160] as well as initial work [161, 162] identifying spin-1/2 Kitaev models on certain three-dimensional, tricoordinated helix lattices.

	other names	Z	inversion	space group	
3D lattices	(10,3)a	hyperoctagon, K4 crystal	4	✗	I <sub>4</sub> 32 214
	(10,3)b	hyperhoneycomb	4	✓	Fddd 70
	(10,3)c	—	6	✗	P3 <sub>1</sub> 12 151
	(9,3)a	—	12	✓	R <sub>3</sub> m 166
	(8,3)a	—	6	✗	P6 <sub>2</sub> 22 180
	(8,3)b	—	6	✓	R <sub>3</sub> m 166
	(8,3)c	—	8	✓	P6 <sub>3</sub> / mmc 194
	(8,3)n	—	16	✓	I <sub>4</sub> / mmm 139
2D	(6,3)	honeycomb	2	✓	

**Table 1:** Overview of tricoordinated lattices in two and three spatial dimensions. Each lattice is described by its Schläfli symbol  $(p, c)$  identifying the length of the elementary loops (or polygonality)  $p$  and tricoordination ( $c = 3$ ). Along with alternative names used in the literature some basic lattice information is provided including the number of sites  $Z$  in the unit cell, an indication whether the lattice exhibits inversion symmetry, and its space group description.

In fact, tricoordinated lattices in three spatial dimensions have been exhaustively classified by Wells in the 1970's [165]. The most elementary ones are lattice structures where all plaquettes (i.e. shortest loops within the lattice) have the *same* length (which is also referred to as the polygonality  $p$  of the lattice). While for two spatial dimensions there is only one such elementary tricoordinated lattice – the honeycomb lattice of polygonality 6, there are multiple elementary lattices of higher polygonality 8, 9, 10 and higher, which are all three-dimensional. An overview of these elementary tricoordinated lattices is given in Table 1, where each lattice is labeled by its Schläfli symbol  $(p, 3)$  and a letter that simply enumerates the lattices for a given Schläfli symbol (the 3 indicates its tricoordination). Fig. 14 illustrates these lattice structures via photographs taken from 3D printed models. For each of these lattice structures there is precisely one assignment of bond-directional Kitaev-type couplings that respects all symmetries of the lattice (up to a trivial permutation among the couplings). The so-defined Kitaev models can all be solved analytically<sup>3</sup> and for all but one lattice, (8,3)n, the ground state is found to be a gapless spin liquid. This state is best described as a *Majorana metal* formed by the itinerant Majorana fermions, while the elementary excitations of the (static)  $Z_2$  gauge field – the visons – are gapped. The precise nature of these Majorana (semi)metals turns out to depend on the underlying lattice geometry and can be captured, e.g. , by its nodal manifold [164]. As described for the hyper-honeycomb (corresponding to the (10,3)b lattice in the above classification) considered by Mandal and Surendran [163], this nodal manifold can be a nodal line. Other possibilities for the nodal structure include the formation of Majorana Fermi surfaces [167] or

<sup>3</sup> In all fairness, it should be noted that this is not entirely true in a rigorous sense. While for the two-dimensional honeycomb model the ground state of the of the  $Z_2$  gauge field can be readily inferred from a theorem of Lieb [166], this is not generically true for the three-dimensional lattices. In fact, only one of the lattices, (8,3)b, strictly allows for the application of the theorem, while for all other lattices one has to resort to alternative means such as numerics. Thus, in a more rigorous sense, only the Kitaev model on lattice (8,3)b can be solved exactly.

	Majorana metal	TR breaking	Peierls instability
3D lattices	(10,3)a	Fermi surface	✓
	(10,3)b	nodal line	✗
	(10,3)c	nodal line	✗
	(9,3)a	Weyl nodes	✗
	(8,3)a	Fermi surface	✓
	(8,3)b	Weyl nodes	✓
	(8,3)c	nodal line	✗
	(8,3)n	gapped	✗
	2D	Dirac nodes	gapped

**Table 2:** Overview of Majorana metals characterizing the gapless spin liquids in three-dimensional Kitaev models. Depending on the underlying lattice geometry, different Majorana (semi)metals are formed by the itinerant Majorana fermions, which are characterized here via their nodal structures. Results for the pure Kitaev model (3) are given in the second column, while the third column provides information on how the metallic nature (and its nodal structure) changes when time-reversal symmetry (TRS) is broken, e.g. by augmenting the Kitaev model by a magnetic field term (pointing along the 111-direction). The last column indicates whether the metallic state is susceptible to a spin-Peierls instability [170]. Table adapted from Ref. [164].

even topologically protected<sup>4</sup> Weyl nodes [168]. Table 2 provides a complete classification of the Majorana metals of all elementary three-dimensional lattices, which notably contains multiple examples each for the emergence of Fermi surfaces, nodal lines, or Weyl nodes for the various lattice structures. For a given lattice, the precise nature of these Majorana metals can in fact be deduced from an elementary symmetry analysis of the projective time-reversal and inversion symmetries as discussed in detail in Ref. [164]. Going beyond these most elementary lattices one might consider, for instance, higher harmonics of a given elementary lattice by systematically enlarging some plaquettes while simultaneously shortening others, see Ref. [101] for further details and showcasing that the stripy-honeycomb lattice is in fact a higher harmonic of the elementary (10,3)b hyper-honeycomb lattice. The classification scheme described above covers all these higher harmonics as well, as the nature of the emergent Majorana metal remains unchanged going from an elementary lattice to any of its higher harmonics<sup>5</sup>.

What does change the nature of the Majorana metal for a given lattice though is the application of a magnetic field or, more generally, the breaking of time-reversal symmetry. For the two-dimensional honeycomb lattice a particularly interesting scenario occurs – the Dirac spin liquid gaps out into a massive non-Abelian topological phase when applying a magnetic field along

<sup>4</sup> The topological nature of the bulk band structure is also reflected in gapless surface states [168, 169, 164] such as Fermi arcs for the Weyl spin liquids.

<sup>5</sup>This excludes the limiting case of the “infinite harmonic”, which in fact is a two-dimensional lattice, e.g. the square-octagon lattice for lattice (10,3)a or the honeycomb lattice for the hyper-honeycomb lattice (10,3)b.

the 111 direction, i.e. a magnetic field that couples to all three spin components

$$H = - \sum_{\gamma-\text{bonds}} K_\gamma S_i^\gamma S_j^\gamma - \sum_j \mathbf{h} \cdot \mathbf{S}_j, \quad (5)$$

with  $\mathbf{h} = h(1, 1, 1)^t$ . Keeping in mind that the Kitaev model reduces to a free (Majorana) fermion model, this scenario can be rationalized by considering the classification of topological insulators [171, 172, 173] rooted in the symmetry classification of free-fermion systems [174]. While the unperturbed Kitaev model resides in symmetry class *BDI*, the model with broken time-reversal symmetry is in symmetry class *D* for which the classification scheme of topological insulators indeed points to the possibility of a topologically non-trivial band insulator in two spatial dimensions. For three spatial dimensions, in contrast, this scenario of driving the (non-interacting) Majorana metal into a topologically non-trivial gapped phase is not possible. Instead, it is found that in the presence of a time-reversal symmetry breaking field (again pointing along the 111-direction), the three-dimensional Kitaev models remain gapless, but the nature of the Majorana metal might change. This is, for instance, the case for the nodal line metals, which in the presence of a magnetic field turn either into Weyl semimetals or Weyl metals, i.e. the energy spectrum acquires Weyl nodes in both cases sitting right at the Fermi energy in the first case and above/below the Fermi energy in the second case [164]. The effect of time-reversal symmetry breaking for all Majorana metals is provided in the third column of Table 2.

Three-dimensional Kitaev models distinguish themselves from their two-dimensional counterparts not only with regard to the variety of possible Majorana metals, but also with regard to the physics of their underlying  $Z_2$  gauge theory. One striking difference between two and three spatial dimensions arises when considering the effect of thermal fluctuations on the order of the  $Z_2$  gauge field. In two spatial dimensions such thermal fluctuations immediately melt the zero-temperature order of the  $Z_2$  gauge field, while for three spatial dimensions it takes a critical strength of the thermal fluctuations to destroy the  $Z_2$  order, i.e. there is a *finite-temperature* transition separating a low-temperature  $Z_2$  ordered state from a high-temperature disordered state. The origin for the absence/occurrence of such a finite-temperature transition in two/three spatial dimensions can readily be understood when considering the nature of defects in the low-temperature  $Z_2$  gauge order. In two spatial dimensions, e.g. for the honeycomb lattice, the elementary excitations are point-like vison excitations (associated with the plaquettes of the honeycomb lattice) that can freely move through the lattice (at no additional energy cost) and thereby thread a flux line through the system which destroys the long-range order of the  $Z_2$  gauge field. For three spatial dimensions, the elementary vison excitations form closed flux *loops*, which leads to a competition between their excitation energy and configurational entropy. As a consequence, it takes a finite temperature to drive the system out of a regime of short flux loops into a regime of extended flux lines, which is connected to the paramagnetic high-temperature regime. In the context of the Kitaev model, this  $Z_2$  gauge physics has been nicely demonstrated [137] via numerically exact quantum Monte Carlo simulations (in the sign-problem free Majorana basis) of the Kitaev model on the hyper-honeycomb (10,3)b lattice. These finite-temperature simulations in fact reveal not only the  $Z_2$  gauge transition at a temperature scale of about  $T \approx 0.004 K$  (where  $K$  is the strength of the Kitaev coupling), but also a thermal cross-over at around  $T \approx 0.6 K$  (i.e. on the bare scale of the Kitaev coupling), which indicates the actual spin fractionalization into Majorana fermions and a  $Z_2$  gauge field, see the specific heat measurements illustrated in Fig. 15.

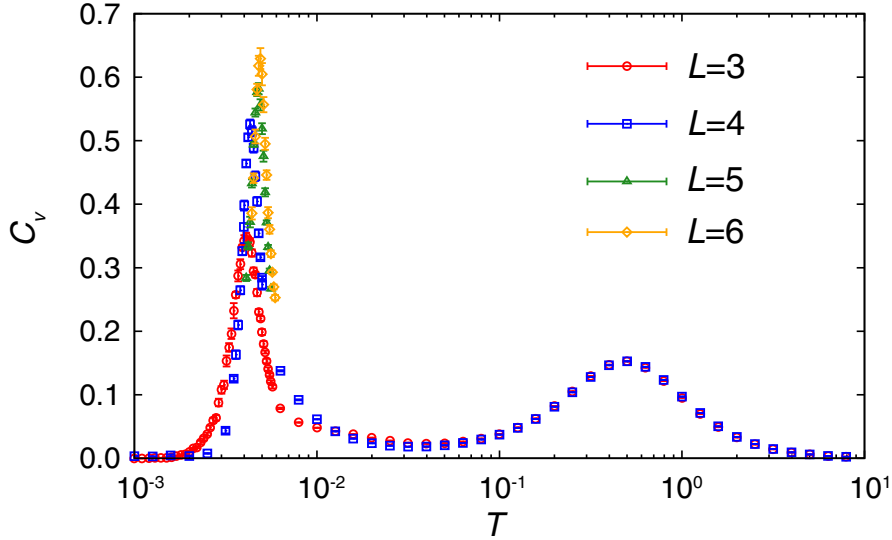


**Fig. 15:** *Signatures of spin fractionalization and a subsequent  $Z_2$  gauge transition in the specific heat calculated for the hyper-honeycomb Kitaev model from numerically exact quantum Monte Carlo simulations [137]. A thermal cross-over indicated by a system-size invariant peak at temperature  $T \approx 0.6$  K (where  $K$  is the strength of the Kitaev coupling) reveals the temperature scale at which the original spin degrees of freedom fractionalize into Majorana fermions and a  $Z_2$  gauge field. The latter undergoes an ordering transition indicated by the (diverging) lower-temperature peak at about  $T \approx 0.004$  K. Figure adapted from Ref. [137].*

The conceptual understanding of three-dimensional Kitaev models has been further expanded by analytical calculations of the dynamical structure factor for the hyper-honeycomb Kitaev model [175] relevant to neutron scattering experiments and the Raman response for both the hyper-honeycomb and stripy-honeycomb Kitaev model [176]. The effects of disorder [177] and interactions [170] have been discussed for some of these lattices with the latter allowing for the possibility of a spin-Peierls instability. For the hyper-honeycomb lattice, extensions of the Kitaev model such as a three-dimensional Heisenberg-Kitaev model [64, 178, 179, 180] and the  $JKT$ -model of Eq. (2) have been considered [181].

Finally, we note that beyond the analytically tractable 3D Kitaev models on tricoordinated lattices other 3D Kitaev generalizations for arbitrary lattice geometries [64] have been considered.

## 4.2 $\beta$ -Li<sub>2</sub>IrO<sub>3</sub> and $\gamma$ -Li<sub>2</sub>IrO<sub>3</sub>

The two Li<sub>2</sub>IrO<sub>3</sub> polymorphs  $\beta$ -Li<sub>2</sub>IrO<sub>3</sub> [100] and  $\gamma$ -Li<sub>2</sub>IrO<sub>3</sub> [101] are the first truly three-dimensional Kitaev materials – realizing as illustrated in Fig. 16 a hyper-honeycomb and stripy-honeycomb lattice of edge-sharing IrO<sub>6</sub> octahedra, respectively. Independently synthesized almost at the same time, they are found to exhibit rather similar physics. Both systems are spin-orbit entangled Mott insulators with effective moments of 1.6(1)  $\mu_B$  close to the value of 1.73  $\mu_B$  for an ideal  $j = 1/2$  moment. Susceptibility fits indicate strong ferromagnetic interactions with estimates of the Curie-Weiss temperature found to be  $\Theta_{\text{CW}} \sim 40$  K ( $\beta$ ) and  $\Theta_{\text{CW}} \sim 75$  K ( $\gamma$ ), respectively. They both order at around  $T_N \sim 38$  K into non-collinear magnetic order. Resonant magnetic x-ray diffraction experiments [182, 183] on about 17 – 100  $\mu\text{m}$  wide single-crystals identify this non-collinear magnetic ordering with non-coplanar, counter-

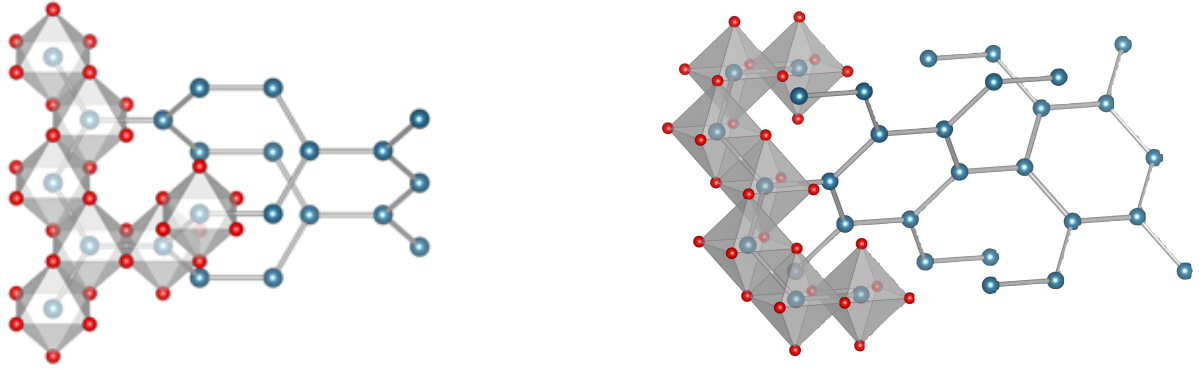


**Fig. 16:** Crystal structure of the hyper-honeycomb Kitaev material  $\beta\text{-Li}_2\text{IrO}_3$  (left) and stripy-honeycomb Kitaev material  $\gamma\text{-Li}_2\text{IrO}_3$  (right).

rotating long range spin spirals with an incommensurate ordering wave vector  $q = (0.57, 0, 0)$  along the orthorhombic  $a$  axis in both materials. This unusual *counter-rotating* spiral order in these three-dimensional  $\text{Li}_2\text{IrO}_3$ -polymorphs is thus very similar to the one (subsequently) observed in the original honeycomb material  $\alpha\text{-Li}_2\text{IrO}_3$ .

From a theoretical perspective, the two three-dimensional  $\text{Li}_2\text{IrO}_3$  polymorphs have been investigated via ab initio calculations supporting the  $j = 1/2$  picture and dominant Kitaev-type bond-directional coupling [184, 185], which for the case of  $\gamma\text{-Li}_2\text{IrO}_3$ , further argue [186] for a reduced symmetry of the local Ir-O-Ir environment (possibly giving rise to rather complex magnetic interactions) to explain the anisotropic behavior observed in optical conductivity measurements [187] for different polarizations. The origin of the magnetic ordering has been scrutinized based on a Heisenberg-Kitaev-Ising model [179, 108] and  $JKT$ -model [178, 181, 109] leading to a unifying theoretical framework [108, 109] for the spiral magnetism in all three  $\text{Li}_2\text{IrO}_3$  polymorphs and their dynamics [188].

More recent experimental studies have argued for evidence of (Majorana) fermion quasiparticles in the Raman scattering [189], employing similar arguments as presented above in some detail for the Raman signatures of  $\alpha\text{-RuCl}_3$ , and the observation that a magnetic field with a small component along the magnetic easy-axis melts the magnetic long-range order, revealing a bistable, strongly correlated spin state [190]. Future high-field experiments will be needed to assert whether this state is indeed a spin liquid. Along similar lines, it will be interesting to pursue high-pressure experiments, which have been argued to drive the three-dimensional Kitaev materials closer to the spin liquid regime [191].

### 4.3 Other materials

We close by mentioning other materials scrutinized as three-dimensional Kitaev materials. This includes a recent theoretical suggestion [192] to synthesize metal-organic compounds such as honeycomb Ru-oxalate frameworks that might realize tricoordinated lattice structures in three spatial dimensions beyond the hyper-honeycomb (and its higher harmonics) such as the (10,3)a hyper-octagon lattice [167]. Further, the Mott insulator  $\text{La}_2\text{B}\text{IrO}_6$  ( $B\text{=Mg,Zn}$ ) has been scrutinized [193, 194] for its  $j = 1/2$  iridium moments being subject to a dominant Kitaev exchange on the face-centered cubic (fcc) lattice. Finally, also the hyperkagome material  $\text{Na}_4\text{Ir}_3\text{O}_8$  [195] has attracted some renewed interest [196, 197] exploring the role of Kitaev-type interactions.

## 5 Outlook

Before taking a look at the road ahead, it is very much worthwhile to note that in the few years since the original 2009 proposal for Kitaev physics in the  $4d^5$  and  $5d^5$  transition metals [9] experimental progress has been made at an incredible pace. Not only have several Kitaev materials with different two- and three-dimensional lattice geometries been synthesized and firmly established as  $j = 1/2$  spin-orbit entangled Mott insulators, but there has also been a streak of impressive experimental findings that most notably have provided direct evidence for bond-directional Kitaev-type interactions [97] in the first Kitaev material  $\text{Na}_2\text{IrO}_3$  and have firmly established the notion of a “proximate spin liquid” in  $\alpha\text{-RuCl}_3$ . This includes the first experimental evidence of fermionic excitations in Raman scattering of a magnetic insulator [135, 136] and a number of highly unusual signatures in inelastic neutron scattering (above the magnetic ordering transition) that can be well attributed to the proximity of spin liquid physics [116, 125]. On the way, the unconventional magnetism of spin-orbit entangled  $j = 1/2$  moments in the  $\text{Li}_2\text{IrO}_3$  polymorphs has been elucidated as a rare example of counter-rotating spin spirals [104].

As the field keeps moving with unflagging momentum, many novel materials are expected to take center stage in the coming years. Within the family of iridates, the hydrogen-intercalated honeycomb material  $\alpha\text{-H}_{3/4}\text{Li}_{1/4}\text{IrO}_3$  [110] will undoubtedly receive much attention for its apparent spin liquid behavior. Beyond the iridates, other  $5d^5$  oxides await experimental scrutiny such as the recently synthesized honeycomb rhodate  $\text{Li}_2\text{RhO}_3$  [198, 199, 200]. The next step might very well be to move beyond oxides altogether, which has already proved judicious with the exploration of the honeycomb chloride  $\alpha\text{-RuCl}_3$ . For instance, the potential for  $j = 1/2$  Mott insulators for iridium and rhenium *fluorides* has been highlighted in recent density functional and dynamical mean field theory studies [201]. In further broadening the search for Kitaev materials, it might also be worthwhile to look beyond  $4d$  and  $5d$  transition metals and consider rare-earth magnets [202] whose  $4f$  electrons are much more localized than the  $5d$  or  $4d$  electrons in iridates and ruthenates and at the same time experience a considerably stronger spin-orbit coupling – thus potentially providing another path to Kitaev materials in the future.

On a conceptual level, interest in Kitaev materials is spurred by their promise to realize what is a truly dichotomous state – a spin-orbit entangled *Mott insulator*, in which the emergent degrees of freedom are Majorana fermions that form an (almost) conventional *metal*. These emergent Majorana metals exhibit distinct (topological) band structures [19, 164] including the formation of Fermi surfaces, nodal lines, and Weyl nodes in three-dimensional settings along with the Dirac nodes of the originally proposed honeycomb system.

### Acknowledgments

The author thanks his various collaborators on Kitaev physics over the years, first and foremost M. Hermanns along with B. Bauer, M. Becker, T. Disselkamp, T. Eschmann, K. O’Brien, M. Garst, M. Gerlach, Z.-C. Gu, H.-C. Jiang, V. Lahtinen, A. W. W. Ludwig, J. K. Pachos, X.-L. Qi, J. Reuther, A. Rosch, E. Sela, and R. Thomale, as well as P. Gegenwart along with experimental collaborators T. Berlijn, W. Ku, S. Manni, and Y. Singh. My group gratefully acknowledges support by the DFG within the CRC 1238 (projects C02, C03).

## References

- [1] Dmytro Pesin and Leon Balents. Mott physics and band topology in materials with strong spin-orbit interaction. *Nat Phys*, 6:376–381, 05 2010.
- [2] M. Z. Hasan and C. L. Kane. *Colloquium* : Topological insulators. *Rev. Mod. Phys.*, 82:3045–3067, Nov 2010.
- [3] Xiao-Liang Qi and Shou-Cheng Zhang. Topological insulators and superconductors. *Rev. Mod. Phys.*, 83:1057–1110, Oct 2011.
- [4] Xiangang Wan, Ari M. Turner, Ashvin Vishwanath, and Sergey Y. Savrasov. Topological semimetal and Fermi-arc surface states in the electronic structure of pyrochlore iridates. *Phys. Rev. B*, 83:205101, May 2011.
- [5] Binghai Yan and Claudia Felser. Topological Materials: Weyl Semimetals. *Annual Review of Condensed Matter Physics*, 8:11.1, 2017.
- [6] William Witczak-Krempa, Gang Chen, Yong Baek Kim, and Leon Balents. Correlated Quantum Phenomena in the Strong Spin-Orbit Regime. *Annual Review of Condensed Matter Physics*, 5:57–82, 2014.
- [7] Giniyat Khaliullin. Orbital Order and Fluctuations in Mott Insulators. *Progress of Theoretical Physics Supplement*, 160:155–202, 2005.
- [8] Gang Chen and Leon Balents. Spin-orbit effects in  $\text{Na}_4\text{Ir}_3\text{O}_8$ : A hyper-kagome lattice antiferromagnet. *Phys. Rev. B*, 78:094403, Sep 2008.
- [9] G. Jackeli and G. Khaliullin. Mott Insulators in the Strong Spin-Orbit Coupling Limit: From Heisenberg to a Quantum Compass and Kitaev Models. *Phys. Rev. Lett.*, 102:017205, Jan 2009.
- [10] B. J. Kim, Hosub Jin, S. J. Moon, J.-Y. Kim, B.-G. Park, C. S. Leem, Jaejun Yu, T. W. Noh, C. Kim, S.-J. Oh, J.-H. Park, V. Durairaj, G. Cao, and E. Rotenberg. Novel  $J_{\text{eff}} = 1/2$  Mott State Induced by Relativistic Spin-Orbit Coupling in  $\text{Sr}_2\text{IrO}_4$ . *Phys. Rev. Lett.*, 101:076402, Aug 2008.
- [11] B. J. Kim, H. Ohsumi, T. Komesu, S. Sakai, T. Morita, H. Takagi, and T. Arima. Phase-Sensitive Observation of a Spin-Orbital Mott State in  $\text{Sr}_2\text{IrO}_4$ . *Science*, 323:1329–1332, 2009.
- [12] Y. K. Kim, O. Krupin, J. D. Denlinger, A. Bostwick, E. Rotenberg, Q. Zhao, J. F. Mitchell, J. W. Allen, and B. J. Kim. Fermi arcs in a doped pseudospin-1/2 Heisenberg antiferromagnet. *Science*, 345:187–190, 2014.
- [13] A. de la Torre, S. McKeown Walker, F. Y. Bruno, S. Riccó, Z. Wang, I. Gutierrez Lezama, G. Scheerer, G. Giriati, D. Jaccard, C. Berthod, T. K. Kim, M. Hoesch, E. C. Hunter, R. S. Perry, A. Tamai, and F. Baumberger. Collapse of the Mott Gap and Emergence of a Nodal Liquid in Lightly Doped  $\text{Sr}_2\text{IrO}_4$ . *Phys. Rev. Lett.*, 115:176402, Oct 2015.

- [14] Yue Cao, Qiang Wang, Justin A. Waugh, Theodore J. Reber, Haoxiang Li, Xiaoqing Zhou, Stephen Parham, S. R. Park, Nicholas C. Plumb, Eli Rotenberg, Aaron Bostwick, Jonathan D. Denlinger, Tongfei Qi, Michael A. Hermele, Gang Cao, and Daniel S. Dessau. Hallmarks of the Mott-metal crossover in the hole-doped pseudospin-1/2 Mott insulator Sr<sub>2</sub>IrO<sub>4</sub>. *Nature Communications*, 7:11367, 04 2016.
- [15] Y. K. Kim, N. H. Sung, J. D. Denlinger, and B. J. Kim. Observation of a d-wave gap in electron-doped Sr<sub>2</sub>IrO<sub>4</sub>. *Nat Phys*, 12:37–41, 01 2016.
- [16] Y. J. Yan, M. Q. Ren, H. C. Xu, B. P. Xie, R. Tao, H. Y. Choi, N. Lee, Y. J. Choi, T. Zhang, and D. L. Feng. Electron-Doped Sr<sub>2</sub>IrO<sub>4</sub>: An Analogue of Hole-Doped Cuprate Superconductors Demonstrated by Scanning Tunneling Microscopy. *Phys. Rev. X*, 5:041018, Nov 2015.
- [17] L. Balents. Spin liquids in frustrated magnets. *Nature*, 464:199, 2010.
- [18] Lucile Savary and Leon Balents. Quantum spin liquids: a review. *Reports on Progress in Physics*, 80:016502, 2017.
- [19] Alexei Kitaev. Anyons in an exactly solved model and beyond. *Annals of Physics*, 321:2 – 111, 2006.
- [20] Zohar Nussinov and Jeroen van den Brink. Compass models: Theory and physical motivations. *Rev. Mod. Phys.*, 87:1–59, Jan 2015.
- [21] Kliment I. Kugel’ and D. I. Khomskii. The Jahn-Teller effect and magnetism: transition metal compounds. *Soviet Physics Uspekhi*, 25:231, 1982.
- [22] Sergey V. Streltsov and Daniel I. Khomskii. Covalent bonds against magnetism in transition metal compounds. *Proceedings of the National Academy of Sciences*, 113:10491–10496, 2016.
- [23] J. Terzic, J. C. Wang, Feng Ye, W. H. Song, S. J. Yuan, S. Aswartham, L. E. DeLong, S. V. Streltsov, D. I. Khomskii, and G. Cao. Coexisting charge and magnetic orders in the dimer-chain iridate Ba<sub>5</sub>AlIr<sub>2</sub>O<sub>11</sub>. *Phys. Rev. B*, 91:235147, Jun 2015.
- [24] Jeffrey G. Rau, Eric Kin-Ho Lee, and Hae-Young Kee. Generic Spin Model for the Honeycomb Iridates beyond the Kitaev Limit. *Phys. Rev. Lett.*, 112:077204, Feb 2014.
- [25] Jeffrey G. Rau, Eric Kin-Ho Lee, and Hae-Young Kee. Spin-Orbit Physics Giving Rise to Novel Phases in Correlated Systems: Iridates and Related Materials. *Annual Review of Condensed Matter Physics*, 7:195–221, 2016.
- [26] Jirí Chaloupka, George Jackeli, and Giniyat Khaliullin. Kitaev-Heisenberg Model on a Honeycomb Lattice: Possible Exotic Phases in Iridium Oxides A<sub>2</sub>IrO<sub>3</sub>. *Phys. Rev. Lett.*, 105:027204, Jul 2010.
- [27] Samarth Chandra, Kabir Ramola, and Deepak Dhar. Classical Heisenberg spins on a hexagonal lattice with Kitaev couplings. *Phys. Rev. E*, 82:031113, Sep 2010.

- [28] Eran Sela, Hong-Chen Jiang, Max H. Gerlach, and Simon Trebst. Order-by-disorder and spin-orbital liquids in a distorted Heisenberg-Kitaev model. *Phys. Rev. B*, 90:035113, Jul 2014.
- [29] Christopher L. Henley. The “Coulomb Phase” in Frustrated Systems. *Annual Review of Condensed Matter Physics*, 1:179, 2010.
- [30] A. Yu. Kitaev. Fault-tolerant quantum computation by anyons. *Annals of Physics*, 303:2 – 30, 2003.
- [31] N. Read and Dmitry Green. Paired states of fermions in two dimensions with breaking of parity and time-reversal symmetries and the fractional quantum Hall effect. *Phys. Rev. B*, 61:10267–10297, Apr 2000.
- [32] Gregory Moore and Nicholas Read. Nonabelions in the fractional quantum Hall effect. *Nuclear Physics B*, 360:362 – 396, 1991.
- [33] Liang Fu and C. L. Kane. Superconducting Proximity Effect and Majorana Fermions at the Surface of a Topological Insulator. *Phys. Rev. Lett.*, 100:096407, Mar 2008.
- [34] Jay D. Sau, Roman M. Lutchyn, Sumanta Tewari, and S. Das Sarma. Generic New Platform for Topological Quantum Computation Using Semiconductor Heterostructures. *Phys. Rev. Lett.*, 104:040502, Jan 2010.
- [35] Jason Alicea, Yuval Oreg, Gil Refael, Felix von Oppen, and Matthew P. A. Fisher. Non-Abelian statistics and topological quantum information processing in 1D wire networks. *Nat Phys*, 7:412–417, 05 2011.
- [36] Roman M. Lutchyn, Jay D. Sau, and S. Das Sarma. Majorana Fermions and a Topological Phase Transition in Semiconductor-Superconductor Heterostructures. *Phys. Rev. Lett.*, 105:077001, Aug 2010.
- [37] Yuval Oreg, Gil Refael, and Felix von Oppen. Helical Liquids and Majorana Bound States in Quantum Wires. *Phys. Rev. Lett.*, 105:177002, Oct 2010.
- [38] Chetan Nayak, Steven H. Simon, Ady Stern, Michael Freedman, and Sankar Das Sarma. Non-abelian anyons and topological quantum computation. *Rev. Mod. Phys.*, 80:1083–1159, Sep 2008.
- [39] Paul E. Lammert, Daniel S. Rokhsar, and John Toner. Topology and nematic ordering. *Phys. Rev. Lett.*, 70:1650–1653, Mar 1993.
- [40] N. Read and Subir Sachdev. Large- $N$  expansion for frustrated quantum antiferromagnets. *Phys. Rev. Lett.*, 66:1773–1776, Apr 1991.
- [41] T. Senthil and Matthew P. A. Fisher.  $Z_2$  gauge theory of electron fractionalization in strongly correlated systems. *Phys. Rev. B*, 62:7850–7881, Sep 2000.
- [42] Xiao-Gang Wen. Quantum orders and symmetric spin liquids. *Phys. Rev. B*, 65:165113, Apr 2002.

- [43] A. J. Willans, J. T. Chalker, and R. Moessner. Disorder in a Quantum Spin Liquid: Flux Binding and Local Moment Formation. *Phys. Rev. Lett.*, 104:237203, Jun 2010.
- [44] A. J. Willans, J. T. Chalker, and R. Moessner. Site dilution in the Kitaev honeycomb model. *Phys. Rev. B*, 84:115146, Sep 2011.
- [45] Eric C. Andrade and Matthias Vojta. Magnetism in spin models for depleted honeycomb-lattice iridates: Spin-glass order towards percolation. *Phys. Rev. B*, 90:205112, Nov 2014.
- [46] Matthias Vojta, Andrew K. Mitchell, and Fabian Zschocke. Kondo Impurities in the Kitaev Spin Liquid: Numerical Renormalization Group Solution and Gauge-Flux-Driven Screening. *Phys. Rev. Lett.*, 117:037202, Jul 2016.
- [47] Ville Lahtinen, Andreas W. W. Ludwig, and Simon Trebst. Perturbed vortex lattices and the stability of nucleated topological phases. *Phys. Rev. B*, 89:085121, Feb 2014.
- [48] Fabian Zschocke and Matthias Vojta. Physical states and finite-size effects in Kitaev's honeycomb model: Bond disorder, spin excitations, and NMR line shape. *Phys. Rev. B*, 92:014403, Jul 2015.
- [49] Stephan Rachel, Lars Fritz, and Matthias Vojta. Landau Levels of Majorana Fermions in a Spin Liquid. *Phys. Rev. Lett.*, 116:167201, Apr 2016.
- [50] Charlotte Gils, Eddy Ardonne, Simon Trebst, Andreas W. W. Ludwig, Matthias Troyer, and Zhenghan Wang. Collective States of Interacting Anyons, Edge States, and the Nucleation of Topological Liquids. *Phys. Rev. Lett.*, 103:070401, Aug 2009.
- [51] Andreas W W Ludwig, Didier Poilblanc, Simon Trebst, and Matthias Troyer. Two-dimensional quantum liquids from interacting non-Abelian anyons. *New Journal of Physics*, 13:045014, 2011.
- [52] Ville Lahtinen, Andreas W. W. Ludwig, Jiannis K. Pachos, and Simon Trebst. Topological liquid nucleation induced by vortex-vortex interactions in Kitaev's honeycomb model. *Phys. Rev. B*, 86:075115, Aug 2012.
- [53] Timo Hyart, Anthony R. Wright, Giniyat Khaliullin, and Bernd Rosenow. Competition between  $d$ -wave and topological  $p$ -wave superconducting phases in the doped Kitaev-Heisenberg model. *Phys. Rev. B*, 85:140510, Apr 2012.
- [54] Yi-Zhuang You, Itamar Kimchi, and Ashvin Vishwanath. Doping a spin-orbit Mott insulator: Topological superconductivity from the Kitaev-Heisenberg model and possible application to  $(\text{Na}_2/\text{Li}_2)\text{IrO}_3$ . *Phys. Rev. B*, 86:085145, Aug 2012.
- [55] Fabien Trouselet, Peter Horsch, Andrzej M. Oleś, and Wen-Long You. Hole propagation in the Kitaev-Heisenberg model: From quasiparticles in quantum Néel states to non-Fermi liquid in the Kitaev phase. *Phys. Rev. B*, 90:024404, Jul 2014.
- [56] Gábor B. Halász, J. T. Chalker, and R. Moessner. Doping a topological quantum spin liquid: Slow holes in the Kitaev honeycomb model. *Phys. Rev. B*, 90:035145, Jul 2014.

- [57] J. Knolle, D. L. Kovrizhin, J. T. Chalker, and R. Moessner. Dynamics of a Two-Dimensional Quantum Spin Liquid: Signatures of Emergent Majorana Fermions and Fluxes. *Phys. Rev. Lett.*, 112:207203, May 2014.
- [58] J. Knolle, D. L. Kovrizhin, J. T. Chalker, and R. Moessner. Dynamics of fractionalization in quantum spin liquids. *Phys. Rev. B*, 92:115127, Sep 2015.
- [59] J. Knolle, Gia-Wei Chern, D. L. Kovrizhin, R. Moessner, and N. B. Perkins. Raman Scattering Signatures of Kitaev Spin Liquids in  $A_2\text{IrO}_3$  Iridates with  $A = \text{Na}$  or  $\text{Li}$ . *Phys. Rev. Lett.*, 113:187201, Oct 2014.
- [60] Brent Perreault, Stephan Rachel, F. J. Burnell, and Johannes Knolle. Majorana Landau Level Raman Spectroscopy, preprint arXiv:1612.03951.
- [61] Brent Perreault, Johannes Knolle, Natalia B. Perkins, and F. J. Burnell. Resonant Raman scattering theory for Kitaev models and their Majorana fermion boundary modes. *Phys. Rev. B*, 94:104427, Sep 2016.
- [62] Gábor B. Halász, Natalia B. Perkins, and Jeroen van den Brink. Resonant Inelastic X-Ray Scattering Response of the Kitaev Honeycomb Model. *Phys. Rev. Lett.*, 117:127203, Sep 2016.
- [63] Jirí Chaloupka, George Jackeli, and Giniyat Khaliullin. Zigzag Magnetic Order in the Iridium Oxide  $\text{Na}_2\text{IrO}_3$ . *Phys. Rev. Lett.*, 110:097204, Feb 2013.
- [64] Itamar Kimchi and Ashvin Vishwanath. Kitaev-Heisenberg models for iridates on the triangular, hyperkagome, kagome, fcc, and pyrochlore lattices. *Phys. Rev. B*, 89:014414, Jan 2014.
- [65] Johannes Reuther, Ronny Thomale, and Simon Trebst. Finite-temperature phase diagram of the Heisenberg-Kitaev model. *Phys. Rev. B*, 84:100406, sep 2011.
- [66] Matthias Gohlke, Ruben Verresen, Roderich Moessner, and Frank Pollmann. Dynamics of the Kitaev-Heisenberg Model, preprint arXiv:1701.04678.
- [67] Hong-Chen Jiang, Zheng-Cheng Gu, Xiao-Liang Qi, and Simon Trebst. Possible proximity of the Mott insulating iridate  $\text{Na}_2\text{IrO}_3$  to a topological phase: Phase diagram of the Heisenberg-Kitaev model in a magnetic field. *Phys. Rev. B*, 83:245104, Jun 2011.
- [68] Itamar Kimchi and Yi-Zhuang You. Kitaev-Heisenberg- $J_2$ - $J_3$  model for the iridates  $A_2\text{IrO}_3$ . *Phys. Rev. B*, 84:180407, Nov 2011.
- [69] Ioannis Rousochatzakis, Johannes Reuther, Ronny Thomale, Stephan Rachel, and N. B. Perkins. Phase Diagram and Quantum Order by Disorder in the Kitaev  $K_1 - K_2$  Honeycomb Magnet. *Phys. Rev. X*, 5:041035, Dec 2015.
- [70] Robert Schaffer, Subhro Bhattacharjee, and Yong Baek Kim. Quantum phase transition in Heisenberg-Kitaev model. *Phys. Rev. B*, 86:224417, Dec 2012.
- [71] Xue-Yang Song, Yi-Zhuang You, and Leon Balents. Low-Energy Spin Dynamics of the Honeycomb Spin Liquid Beyond the Kitaev Limit. *Phys. Rev. Lett.*, 117:037209, Jul 2016.

- [72] Joji Nasu, Yasuyuki Kato, Junki Yoshitake, Yoshitomo Kamiya, and Yukitoshi Motome. Liquid-Liquid Transition in Kitaev Magnets Driven by Spin Fractionalization, preprint arXiv:1610.07343.
- [73] Manuel Laubach, Johannes Reuther, Ronny Thomale, and Stephan Rachel. Three-band Hubbard model for  $\text{Na}_2\text{IrO}_3$ : Topological insulator, zigzag antiferromagnet, and Kitaev-Heisenberg material, preprint arXiv:1701.04896.
- [74] Craig C. Price and Natalia B. Perkins. Critical Properties of the Kitaev-Heisenberg Model. *Phys. Rev. Lett.*, 109:187201, Nov 2012.
- [75] Craig Price and Natalia B. Perkins. Finite-temperature phase diagram of the classical Kitaev-Heisenberg model. *Phys. Rev. B*, 88:024410, Jul 2013.
- [76] Lukas Janssen, Eric C. Andrade, and Matthias Vojta. Honeycomb-Lattice Heisenberg-Kitaev Model in a Magnetic Field: Spin Canting, Metamagnetism, and Vortex Crystals. *Phys. Rev. Lett.*, 117:277202, Dec 2016.
- [77] Gia-Wei Chern, Yuriy Sizuk, Craig Price, and Natalia B. Perkins. Kitaev-Heisenberg model in a magnetic field: order-by-disorder and commensurate-incommensurate transitions, preprint arXiv:1611.03436.
- [78] H. Takagi. private communication, 2009.
- [79] Yogesh Singh and P. Gegenwart. Antiferromagnetic Mott insulating state in single crystals of the honeycomb lattice material  $\text{Na}_2\text{IrO}_3$ . *Phys. Rev. B*, 82:064412, Aug 2010.
- [80] Atsuo Shitade, Hosho Katsura, Jan Kuneš, Xiao-Liang Qi, Shou-Cheng Zhang, and Naoto Nagaosa. Quantum Spin Hall Effect in a Transition Metal Oxide  $\text{Na}_2\text{IrO}_3$ . *Phys. Rev. Lett.*, 102:256403, Jun 2009.
- [81] Feng Ye, Songxue Chi, Huibo Cao, Bryan C. Chakoumakos, Jaime A. Fernandez-Baca, Radu Custelcean, T. F. Qi, O. B. Korneta, and G. Cao. Direct evidence of a zigzag spin-chain structure in the honeycomb lattice: A neutron and x-ray diffraction investigation of single-crystal  $\text{Na}_2\text{IrO}_3$ . *Phys. Rev. B*, 85:180403, May 2012.
- [82] R. Comin, G. Levy, B. Ludbrook, Z.-H. Zhu, C. N. Veenstra, J. A. Rosen, Yogesh Singh, P. Gegenwart, D. Stricker, J. N. Hancock, D. van der Marel, I. S. Elfimov, and A. Damascelli.  $\text{Na}_2\text{IrO}_3$  as a Novel Relativistic Mott Insulator with a 340-meV Gap. *Phys. Rev. Lett.*, 109:266406, Dec 2012.
- [83] Yogesh Singh, S. Manni, J. Reuther, T. Berlijn, R. Thomale, W. Ku, S. Trebst, and P. Gegenwart. Relevance of the Heisenberg-Kitaev Model for the Honeycomb Lattice Iridates  $\text{A}_2\text{IrO}_3$ . *Phys. Rev. Lett.*, 108:127203, mar 2012.
- [84] C. H. Sohn, H.-S. Kim, T. F. Qi, D. W. Jeong, H. J. Park, H. K. Yoo, H. H. Kim, J.-Y. Kim, T. D. Kang, Deok-Yong Cho, G. Cao, J. Yu, S. J. Moon, and T. W. Noh. Mixing between  $J_{\text{eff}} = \frac{1}{2}$  and  $\frac{3}{2}$  orbitals in  $\text{Na}_2\text{IrO}_3$ : A spectroscopic and density functional calculation study. *Phys. Rev. B*, 88:085125, Aug 2013.

- [85] H. Gretarsson, J. P. Clancy, X. Liu, J. P. Hill, Emil Bozin, Yogesh Singh, S. Manni, P. Gegenwart, Jungho Kim, A. H. Said, D. Casa, T. Gog, M. H. Upton, Heung-Sik Kim, J. Yu, Vamshi M. Katukuri, L. Hozoi, Jeroen van den Brink, and Young-June Kim. Crystal-Field Splitting and Correlation Effect on the Electronic Structure of  $A_2\text{IrO}_3$ . *Phys. Rev. Lett.*, 110:076402, Feb 2013.
- [86] H. Gretarsson, J. P. Clancy, Yogesh Singh, P. Gegenwart, J. P. Hill, Jungho Kim, M. H. Upton, A. H. Said, D. Casa, T. Gog, and Young-June Kim. Magnetic excitation spectrum of  $\text{Na}_2\text{IrO}_3$  probed with resonant inelastic x-ray scattering. *Phys. Rev. B*, 87:220407, Jun 2013.
- [87] B. Andlauer, J. Schneider, and W. Tolksdorf. Optical Absorption, Fluorescence, and Electron Spin Resonance of  $\text{Ir}^{4+}$  on Octahedral Sites in  $\text{Y}_3\text{Ga}_5\text{O}_{12}$ . *Physica status solidi (b)*, 73:533–540, 1976.
- [88] K.W. Blazey and F. Levy. EPR of rhodium, osmium and iridium-doped rutile. *Solid State Communications*, 59:335 – 338, 1986.
- [89] X. Liu, T. Berlijn, W.-G. Yin, W. Ku, A. Tsvelik, Young-June Kim, H. Gretarsson, Yogesh Singh, P. Gegenwart, and J. P. Hill. Long-range magnetic ordering in  $\text{Na}_2\text{IrO}_3$ . *Phys. Rev. B*, 83:220403, Jun 2011.
- [90] S. K. Choi, R. Coldea, A. N. Kolmogorov, T. Lancaster, I. I. Mazin, S. J. Blundell, P. G. Radaelli, Yogesh Singh, P. Gegenwart, K. R. Choi, S.-W. Cheong, P. J. Baker, C. Stock, and J. Taylor. Spin Waves and Revised Crystal Structure of Honeycomb Iridate  $\text{Na}_2\text{IrO}_3$ . *Phys. Rev. Lett.*, 108:127204, Mar 2012.
- [91] Yuriy Sizyuk, Craig Price, Peter Wölfle, and Natalia B. Perkins. Importance of anisotropic exchange interactions in honeycomb iridates: Minimal model for zigzag antiferromagnetic order in  $\text{Na}_2\text{IrO}_3$ . *Phys. Rev. B*, 90:155126, Oct 2014.
- [92] Yuriy Sizyuk, Peter Wölfle, and Natalia B. Perkins. Selection of direction of the ordered moments in  $\text{Na}_2\text{IrO}_3$  and  $\alpha - \text{RuCl}_3$ . *Phys. Rev. B*, 94:085109, Aug 2016.
- [93] I. I. Mazin, Harald O. Jeschke, Kateryna Foyevtsova, Roser Valentí, and D. I. Khomskii.  $\text{Na}_2\text{IrO}_3$  as a Molecular Orbital Crystal. *Phys. Rev. Lett.*, 109:197201, Nov 2012.
- [94] Kateryna Foyevtsova, Harald O. Jeschke, I. I. Mazin, D. I. Khomskii, and Roser Valentí. *Ab initio* analysis of the tight-binding parameters and magnetic interactions in  $\text{Na}_2\text{IrO}_3$ . *Phys. Rev. B*, 88:035107, Jul 2013.
- [95] I. I. Mazin, S. Manni, K. Foyevtsova, Harald O. Jeschke, P. Gegenwart, and Roser Valentí. Origin of the insulating state in honeycomb iridates and rhodates. *Phys. Rev. B*, 88:035115, Jul 2013.
- [96] Junki Yoshitake, Joji Nasu, and Yukitoshi Motome. Fractional Spin Fluctuations as a Precursor of Quantum Spin Liquids: Majorana Dynamical Mean-Field Study for the Kitaev Model. *Phys. Rev. Lett.*, 117:157203, Oct 2016.

- [97] Sae Hwan Chun, Jong-Woo Kim, Jungho Kim, H. Zheng, Constantinos C. Stoumpos, C. D. Malliakas, J. F. Mitchell, Kavita Mehlawat, Yogesh Singh, Y. Choi, T. Gog, A. Al-Zein, M. Moretti Sala, M. Krisch, J. Chaloupka, G. Jackeli, G. Khaliullin, and B. J. Kim. Direct evidence for dominant bond-directional interactions in a honeycomb lattice iridate  $\text{Na}_2\text{IrO}_3$ . *Nat Phys*, 11:462–466, 06 2015.
- [98] Youhei Yamaji, Takafumi Suzuki, Takuto Yamada, Sei-ichiro Suga, Naoki Kawashima, and Masatoshi Imada. Clues and criteria for designing a Kitaev spin liquid revealed by thermal and spin excitations of the honeycomb iridate  $\text{Na}_2\text{IrO}_3$ . *Phys. Rev. B*, 93:174425, May 2016.
- [99] Stephen M. Winter, Ying Li, Harald O. Jeschke, and Roser Valentí. Challenges in design of Kitaev materials: Magnetic interactions from competing energy scales. *Phys. Rev. B*, 93:214431, Jun 2016.
- [100] T. Takayama, A. Kato, R. Dinnebier, J. Nuss, H. Kono, L. S. I. Veiga, G. Fabbris, D. Haskel, and H. Takagi. Hyperhoneycomb Iridate  $\beta\text{-Li}_2\text{IrO}_3$  as a Platform for Kitaev Magnetism. *Phys. Rev. Lett.*, 114:077202, Feb 2015.
- [101] K. A. Modic, Tess E. Smidt, Itamar Kimchi, Nicholas P. Breznay, Alun Biffin, Sungkyun Choi, Roger D. Johnson, Radu Coldea, Pilanda Watkins-Curry, Gregory T. McCandless, Julia Y. Chan, Felipe Gandara, Z. Islam, Ashvin Vishwanath, Arkady Shekhter, Ross D. McDonald, and James G. Analytis. Realization of a three-dimensional spin-anisotropic harmonic honeycomb iridate. *Nature Communications*, 5:4203, 06 2014.
- [102] Marcus Jenderka, Rüdiger Schmidt-Grund, Marius Grundmann, and Michael Lorenz. Electronic excitations and structure of  $\text{Li}_2\text{IrO}_3$  thin films grown on  $\text{ZrO}_2:\text{Y}$  (001) substrates. *Journal of Applied Physics*, 117:025304, 2015.
- [103] F. Freund, S. C. Williams, R. D. Johnson, R. Coldea, P. Gegenwart, and A. Jesche. Single crystal growth from separated educts and its application to lithium transition-metal oxides. *Scientific Reports*, 6:35362, Oct 2016.
- [104] S. C. Williams, R. D. Johnson, F. Freund, Sungkyun Choi, A. Jesche, I. Kimchi, S. Manni, A. Bombardi, P. Manuel, P. Gegenwart, and R. Coldea. Incommensurate counterrotating magnetic order stabilized by Kitaev interactions in the layered honeycomb  $\alpha\text{-Li}_2\text{IrO}_3$ . *Phys. Rev. B*, 93:195158, May 2016.
- [105] Johannes Reuther, Ronny Thomale, and Stephan Rachel. Spiral order in the honeycomb iridate  $\text{Li}_2\text{IrO}_3$ . *Phys. Rev. B*, 90:100405, Sep 2014.
- [106] Jiri Chaloupka and Giniyat Khaliullin. Hidden symmetries of the extended Kitaev-Heisenberg model: Implications for the honeycomb-lattice iridates  $A_2\text{IrO}_3$ . *Phys. Rev. B*, 92:024413, Jul 2015.
- [107] Satoshi Nishimoto, Vamshi M. Katukuri, Viktor Yushankhai, Hermann Stoll, Ulrich K. Rößler, Liviu Hozoi, Ioannis Rousochatzakis, and Jeroen van den Brink. Strongly frustrated triangular spin lattice emerging from triplet dimer formation in honeycomb  $\text{Li}_2\text{IrO}_3$ . *Nature Communications*, 7:10273, 01 2016.

- [108] Itamar Kimchi, Radu Coldea, and Ashvin Vishwanath. Unified theory of spiral magnetism in the harmonic-honeycomb iridates  $\alpha$ ,  $\beta$ , and  $\gamma$   $\text{Li}_2\text{IrO}_3$ . *Phys. Rev. B*, 91:245134, Jun 2015.
- [109] Eric Kin-Ho Lee, Jeffrey G. Rau, and Yong Baek Kim. Two iridates, two models, and two approaches: A comparative study on magnetism in three-dimensional honeycomb materials. *Phys. Rev. B*, 93:184420, May 2016.
- [110] H. Takagi. Opening colloquium of CRC 1283 “Control and Dynamics of Quantum Materials”, University of Cologne, October 2016.
- [111] L. Binotto, I. Pollini, and G. Spinolo. Optical and transport properties of the magnetic semiconductor  $\alpha$ - $\text{RuCl}_3$ . *Physica Status Solidi (b)*, 44:245–252, 1971.
- [112] I. Pollini. Electronic properties of the narrow-band material  $\alpha$ - $\text{RuCl}_3$ . *Phys. Rev. B*, 53:12769–12776, May 1996.
- [113] K. W. Plumb, J. P. Clancy, L. J. Sandilands, V. Vijay Shankar, Y. F. Hu, K. S. Burch, Hae-Young Kee, and Young-June Kim.  $\alpha$  –  $\text{RuCl}_3$ : A spin-orbit assisted Mott insulator on a honeycomb lattice. *Phys. Rev. B*, 90:041112, Jul 2014.
- [114] Xiaoqing Zhou, Haoxiang Li, J. A. Waugh, S. Parham, Heung-Sik Kim, J. A. Sears, A. Gomes, Hae-Young Kee, Young-June Kim, and D. S. Dessau. Angle-resolved photoemission study of the Kitaev candidate  $\alpha$  –  $\text{RuCl}_3$ . *Phys. Rev. B*, 94:161106, Oct 2016.
- [115] Luke J. Sandilands, Yao Tian, Anjan A. Reijnders, Heung-Sik Kim, K. W. Plumb, Young-June Kim, Hae-Young Kee, and Kenneth S. Burch. Spin-orbit excitations and electronic structure of the putative Kitaev magnet  $\alpha$  –  $\text{RuCl}_3$ . *Phys. Rev. B*, 93:075144, Feb 2016.
- [116] A. Banerjee, C. A. Bridges, J. Q. Yan, A. A. Acczel, L. Li, M. B. Stone, G. E. Granroth, M. D. Lumsden, Y. Yiu, J. Knolle, S. Bhattacharjee, D. L. Kovrizhin, R. Moessner, D. A. Tennant, D. G. Mandrus, and S. E. Nagler. Proximate kитаев quantum spin liquid behaviour in a honeycomb magnet. *Nat Mater*, 15:733–740, 07 2016.
- [117] B. N. Figgis, J. Lewis, F. E. Mabbs, and G. A. Webb. Magnetic properties of some iron(iii) and ruthenium(iii) low-spin complexes. *J. Chem. Soc. A*, pages 422–426, 1966.
- [118] Y. Kobayashi, T. Okada, K. Asai, M. Katada, H. Sano, and F. Ambe. Moessbauer spectroscopy and magnetization studies of .alpha.- and .beta.-ruthenium trichloride. *Inorganic Chemistry*, 31:4570–4574, 1992.
- [119] J. M. Fletcher, W. E. Gardner, A. C. Fox, and G. Topping. X-ray, infrared, and magnetic studies of  $\alpha$ - and  $\beta$ -ruthenium trichloride. *J. Chem. Soc. A*, pages 1038–1045, 1967.
- [120] A. Koitzsch, C. Habenicht, E. Müller, M. Knupfer, B. Büchner, H. C. Kandpal, J. van den Brink, D. Nowak, A. Isaeva, and Th. Doert.  $J_{\text{eff}}$  Description of the Honeycomb Mott Insulator  $\alpha$ - $\text{RuCl}_3$ . *Phys. Rev. Lett.*, 117:126403, Sep 2016.
- [121] Soobin Sinn, Choong Hyun Kim, Beom Hyun Kim, Kyung Dong Lee, Choong Jae Won, Ji Seop Oh, Moonsup Han, Young Jun Chang, Namjung Hur, Hitoshi Sato, Byeong-Gyu Park, Changyoung Kim, Hyeong-Do Kim, and Tae Won Noh. Electronic Structure

- of the Kitaev Material  $\alpha$ -RuCl<sub>3</sub> Probed by Photoemission and Inverse Photoemission Spectroscopies. *Scientific Reports*, 6:39544, Dec 2016.
- [122] M. Ziatdinov, A. Banerjee, A. Maksov, T. Berlijn, W. Zhou, H. B. Cao, J. Q. Yan, C. A. Bridges, D. G. Mandrus, S. E. Nagler, A. P. Baddorf, and S. V. Kalinin. Atomic-scale observation of structural and electronic orders in the layered compound  $\alpha$ -RuCl<sub>3</sub>. *Nature Communications*, 7:13774, 12 2016.
- [123] M. Majumder, M. Schmidt, H. Rosner, A. A. Tsirlin, H. Yasuoka, and M. Baenitz. Anisotropic Ru<sup>3+</sup>4d<sup>5</sup> magnetism in the  $\alpha$ -RuCl<sub>3</sub> honeycomb system: Susceptibility, specific heat, and zero-field NMR. *Phys. Rev. B*, 91:180401, May 2015.
- [124] H. B. Cao, A. Banerjee, J.-Q. Yan, C. A. Bridges, M. D. Lumsden, D. G. Mandrus, D. A. Tennant, B. C. Chakoumakos, and S. E. Nagler. Low-temperature crystal and magnetic structure of  $\alpha$ -RuCl<sub>3</sub>. *Phys. Rev. B*, 93:134423, Apr 2016.
- [125] Arnab Banerjee, Jiaqiang Yan, Johannes Knolle, Craig A. Bridges, Matthew B. Stone, Mark D. Lumsden, David G. Mandrus, David A. Tennant, Roderich Moessner, and Stephen E. Nagler. Neutron tomography of magnetic Majorana fermions in a proximate quantum spin liquid, preprint arXiv:1609.00103.
- [126] J. A. Sears, M. Songvilay, K. W. Plumb, J. P. Clancy, Y. Qiu, Y. Zhao, D. Parshall, and Young-June Kim. Magnetic order in  $\alpha$ -RuCl<sub>3</sub>: A honeycomb-lattice quantum magnet with strong spin-orbit coupling. *Phys. Rev. B*, 91:144420, Apr 2015.
- [127] C. Ritter. Zigzag type magnetic structure of the spin  $J_{\text{eff}} = 1/2$  compound  $\alpha$ -RuCl<sub>3</sub> as determined by neutron powder diffraction. *Journal of Physics: Conference Series*, 746:012060, 2016.
- [128] R. D. Johnson, S. C. Williams, A. A. Haghishirad, J. Singleton, V. Zapf, P. Manuel, I. I. Mazin, Y. Li, H. O. Jeschke, R. Valentí, and R. Coldea. Monoclinic crystal structure of  $\alpha$ -RuCl<sub>3</sub> and the zigzag antiferromagnetic ground state. *Phys. Rev. B*, 92:235119, Dec 2015.
- [129] F. Lang, P. J. Baker, A. A. Haghishirad, Y. Li, D. Prabhakaran, R. Valentí, and S. J. Blundell. Unconventional magnetism on a honeycomb lattice in  $\alpha$ -RuCl<sub>3</sub> studied by muon spin rotation. *Phys. Rev. B*, 94:020407, Jul 2016.
- [130] Heung-Sik Kim, Vijay Shankar V., Andrei Catuneanu, and Hae-Young Kee. Kitaev magnetism in honeycomb RuCl<sub>3</sub> with intermediate spin-orbit coupling. *Phys. Rev. B*, 91:241110, Jun 2015.
- [131] Heung-Sik Kim and Hae-Young Kee. Crystal structure and magnetism in  $\alpha$ -RuCl<sub>3</sub>: An *ab initio* study. *Phys. Rev. B*, 93:155143, Apr 2016.
- [132] Ravi Yadav, Nikolay A. Bogdanov, Vamshi M. Katukuri, Satoshi Nishimoto, Jeroen van den Brink, and Liviu Hozoi. Kitaev exchange and field-induced quantum spin-liquid states in honeycomb  $\alpha$ -RuCl<sub>3</sub>. *Scientific Reports*, 6:37925, Nov 2016.
- [133] Jirí Chaloupka and Giniyat Khaliullin. Magnetic anisotropy in the Kitaev model systems Na<sub>2</sub>IrO<sub>3</sub> and RuCl<sub>3</sub>. *Phys. Rev. B*, 94:064435, Aug 2016.

- [134] Daichi Hirobe, Masahiro Sato, Yuki Shiomi, Hidekazu Tanaka, and Eiji Saitoh. Magnetic thermal conductivity far above the Nel temperatures in the Kitaev-magnet candidate  $\alpha$ -RuCl<sub>3</sub>, preprint arXiv:1611.04799.
- [135] Luke J. Sandilands, Yao Tian, Kemp W. Plumb, Young-June Kim, and Kenneth S. Burch. Scattering Continuum and Possible Fractionalized Excitations in  $\alpha$ -RuCl<sub>3</sub>. *Phys. Rev. Lett.*, 114:147201, Apr 2015.
- [136] J. Nasu, J. Knolle, D. L. Kovrizhin, Y. Motome, and R. Moessner. Fermionic response from fractionalization in an insulating two-dimensional magnet. *Nat Phys*, 12:912–915, 10 2016.
- [137] Joji Nasu, Masafumi Udagawa, and Yukitoshi Motome. Vaporization of Kitaev Spin Liquids. *Phys. Rev. Lett.*, 113:197205, 2014.
- [138] Luke J. Sandilands, C. H. Sohn, H. J. Park, So Yeun Kim, K. W. Kim, Jennifer A. Sears, Young-June Kim, and Tae Won Noh. Optical probe of Heisenberg-Kitaev magnetism in  $\alpha$ -RuCl<sub>3</sub>. *Phys. Rev. B*, 94:195156, Nov 2016.
- [139] Tusharkanti Dey, A. V. Mahajan, P. Khuntia, M. Baenitz, B. Koteswararao, and F. C. Chou. Spin-liquid behavior in  $J_{\text{eff}} = \frac{1}{2}$  triangular lattice compound Ba<sub>3</sub>IrTi<sub>2</sub>O<sub>9</sub>. *Phys. Rev. B*, 86:140405, Oct 2012.
- [140] Takeshi Sakamoto, Yoshihiro Doi, and Yukio Hinatsu. Crystal structures and magnetic properties of 6H-perovskite-type oxides Ba<sub>3</sub>MIr<sub>2</sub>O<sub>9</sub> (M=Mg, Ca, Sc, Ti, Zn, Sr, Zr, Cd and In). *Journal of Solid State Chemistry*, 179:2595 – 2601, 2006.
- [141] Michael Becker, Maria Hermanns, Bela Bauer, Markus Garst, and Simon Trebst. Spin-orbit physics of  $j = \frac{1}{2}$  Mott insulators on the triangular lattice. *Phys. Rev. B*, 91:155135, Apr 2015.
- [142] Ioannis Rousochatzakis, Ulrich K. Rössler, Jeroen van den Brink, and Maria Daghofer. Kitaev anisotropy induces mesoscopic  $\mathbb{Z}_2$  vortex crystals in frustrated hexagonal antiferromagnets. *Phys. Rev. B*, 93:104417, Mar 2016.
- [143] R. Kumar, D. Sheptyakov, P. Khuntia, K. Rolfs, P. G. Freeman, H. M. Rønnow, Tusharkanti Dey, M. Baenitz, and A. V. Mahajan. Ba<sub>3</sub>M<sub>x</sub>Ti<sub>3-x</sub>O<sub>9</sub> (M = Ir, Rh): A family of 5d/4d-based diluted quantum spin liquids. *Phys. Rev. B*, 94:174410, Nov 2016.
- [144] Andrei Catuneanu, Jeffrey G. Rau, Heung-Sik Kim, and Hae-Young Kee. Magnetic orders proximal to the Kitaev limit in frustrated triangular systems: Application to Ba<sub>3</sub>IrTi<sub>2</sub>O<sub>9</sub>. *Phys. Rev. B*, 92:165108, Oct 2015.
- [145] Kai Li, Shun-Li Yu, and Jian-Xin Li. Global phase diagram, possible chiral spin liquid, and topological superconductivity in the triangular Kitaev-Heisenberg model. *New Journal of Physics*, 17:043032, 2015.
- [146] Pavel Kos and Matthias Punk. Quantum spin liquid ground states of the Heisenberg-Kitaev model on the triangular lattice, preprint arXiv:1611.05454.

- [147] Kazuya Shinjo, Shigetoshi Sota, Seiji Yunoki, Keisuke Totsuka, and Takami Tohyama. Density-Matrix Renormalization Group Study of KitaevHeisenberg Model on a Triangular Lattice. *Journal of the Physical Society of Japan*, 85:114710, 2016.
- [148] Tsuyoshi Okubo, Sungki Chung, and Hikaru Kawamura. Multiple- $q$  States and the Skyrmiion Lattice of the Triangular-Lattice Heisenberg Antiferromagnet under Magnetic Fields. *Phys. Rev. Lett.*, 108:017206, Jan 2012.
- [149] H. D. Rosales, D. C. Cabra, and Pierre Pujol. Three-sublattice skyrmion crystal in the antiferromagnetic triangular lattice. *Phys. Rev. B*, 92:214439, Dec 2015.
- [150] Tusharkanti Dey, A. V. Mahajan, R. Kumar, B. Koteswararao, F. C. Chou, A. A. Omrani, and H. M. Ronnow. Possible spin-orbit driven spin-liquid ground state in the double perovskite phase of  $\text{Ba}_3\text{YIr}_2\text{O}_9$ . *Phys. Rev. B*, 88:134425, Oct 2013.
- [151] Tusharkanti Dey, R. Kumar, A. V. Mahajan, S. D. Kaushik, and V. Siruguri. Unconventional magnetism in the spin-orbit-driven Mott insulators  $\text{Ba}_3M\text{Ir}_2\text{O}_9$  ( $M = \text{Sc}, \text{Y}$ ). *Phys. Rev. B*, 89:205101, May 2014.
- [152] Tusharkanti Dey. CRC 1238 colloquium, Cologne, October 2016.
- [153] Ichiro Terasaki, Taichi Igarashi, Takayuki Nagai, Kenji Tanabe, Hiroki Taniguchi, Taku Matsushita, Nobuo Wada, Atsushi Takata, Takanori Kida, Masayuki Hagiwara, Kensuke Kobayashi, Hajime Sagayama, Reiji Kumai, Hironori Nakao, and Youichi Murakami. Absence of magnetic long range order in  $\text{Ba}_3\text{ZnRu}_2\text{O}_9$ : A spin-liquid candidate in the  $S = 3/2$  dimer lattice, preprint arXiv:1701.02257.
- [154] Hong Yao and Steven A. Kivelson. Exact Chiral Spin Liquid with Non-Abelian Anyons. *Phys. Rev. Lett.*, 99:247203, Dec 2007.
- [155] V. Kalmeyer and R. B. Laughlin. Equivalence of the resonating-valence-bond and fractional quantum Hall states. *Phys. Rev. Lett.*, 59:2095–2098, Nov 1987.
- [156] B. Bauer, L. Cincio, B. P. Keller, M. Dolfi, G. Vidal, S. Trebst, and A. W. W. Ludwig. Chiral spin liquid and emergent anyons in a Kagome lattice Mott insulators. *Nature Commun.*, 5:5137, 2014.
- [157] Yin-Chen He, D. N. Sheng, and Yan Chen. Chiral Spin Liquid in a Frustrated Anisotropic Kagome Heisenberg Model. *Phys. Rev. Lett.*, 112:137202, Apr 2014.
- [158] Shou-Shu Gong, Wei Zhu, and D. N. Sheng. Emergent Chiral Spin Liquid: Fractional Quantum Hall Effect in a Kagome Heisenberg Model. *Scientific Reports*, May:6317, 2014.
- [159] Shou-Shu Gong, Wei Zhu, Leon Balents, and D. N. Sheng. Global phase diagram of competing ordered and quantum spin-liquid phases on the kagome lattice. *Phys. Rev. B*, 91:075112, Feb 2015.
- [160] Shinsei Ryu. Three-dimensional topological phase on the diamond lattice. *Phys. Rev. B*, 79:075124, Feb 2009.

- [161] Tieyan Si and Yue Yu. Exactly soluble spin-1/2 models on three-dimensional lattices and non-abelian statistics of closed string excitations, preprint arXiv:0709.1302.
- [162] Tieyan Si and Yue Yu. Anyonic loops in three-dimensional spin liquid and chiral spin liquid. *Nuclear Physics B*, 803:428 – 449, 2008.
- [163] Saptarshi Mandal and Naveen Surendran. Exactly solvable Kitaev model in three dimensions. *Phys. Rev. B*, 79:024426, Jan 2009.
- [164] Kevin O'Brien, Maria Hermanns, and Simon Trebst. Classification of gapless  $\mathbb{Z}_2$  spin liquids in three-dimensional Kitaev models. *Phys. Rev. B*, 93:085101, Feb 2016.
- [165] A. F. Wells. *Three-Dimensional Nets and Polyhedra*. Wiley, New York, 1977.
- [166] Elliott H. Lieb. Flux Phase of the Half-Filled Band. *Phys. Rev. Lett.*, 73:2158–2161, Oct 1994.
- [167] M. Hermanns and S. Trebst. Quantum spin liquid with a Majorana Fermi surface on the three-dimensional hyperoctagon lattice. *Phys. Rev. B*, 89:235102, Jun 2014.
- [168] M. Hermanns, K. O'Brien, and S. Trebst. Weyl Spin Liquids. *Phys. Rev. Lett.*, 114:157202, Apr 2015.
- [169] Robert Schaffer, Eric Kin-Ho Lee, Yuan-Ming Lu, and Yong Baek Kim. Topological Spinon Semimetals and Gapless Boundary States in Three Dimensions. *Phys. Rev. Lett.*, 114:116803, Mar 2015.
- [170] Maria Hermanns, Simon Trebst, and Achim Rosch. Spin-Peierls Instability of Three-Dimensional Spin Liquids with Majorana Fermi Surfaces. *Phys. Rev. Lett.*, 115:177205, Oct 2015.
- [171] Andreas P. Schnyder, Shinsei Ryu, Akira Furusaki, and Andreas W. W. Ludwig. Classification of topological insulators and superconductors in three spatial dimensions. *Phys. Rev. B*, 78:195125, Nov 2008.
- [172] Alexei Kitaev. Periodic table for topological insulators and superconductors. *AIP Conference Proceedings*, 1134:22–30, 2009.
- [173] Shinsei Ryu, Andreas P Schnyder, Akira Furusaki, and Andreas W W Ludwig. Topological insulators and superconductors: tenfold way and dimensional hierarchy. *New Journal of Physics*, 12:065010, 2010.
- [174] Alexander Altland and Martin R. Zirnbauer. Nonstandard symmetry classes in mesoscopic normal-superconducting hybrid structures. *Phys. Rev. B*, 55:1142–1161, Jan 1997.
- [175] A. Smith, J. Knolle, D. L. Kovrizhin, J. T. Chalker, and R. Moessner. Neutron scattering signatures of the 3D hyperhoneycomb Kitaev quantum spin liquid. *Phys. Rev. B*, 92:180408, Nov 2015.
- [176] Brent Perreault, Johannes Knolle, Natalia B. Perkins, and F. J. Burnell. Theory of Raman response in three-dimensional Kitaev spin liquids: Application to  $\beta$ - and  $\gamma$  –  $\text{Li}_2\text{IrO}_3$  compounds. *Phys. Rev. B*, 92:094439, Sep 2015.

- [177] G. J. Sreejith, Subhro Bhattacharjee, and R. Moessner. Vacancies in Kitaev quantum spin liquids on the three-dimensional hyperhoneycomb lattice. *Phys. Rev. B*, 93:064433, Feb 2016.
- [178] Eric Kin-Ho Lee, Robert Schaffer, Subhro Bhattacharjee, and Yong Baek Kim. Heisenberg-Kitaev model on the hyperhoneycomb lattice. *Phys. Rev. B*, 89:045117, Jan 2014.
- [179] Itamar Kimchi, James G. Analytis, and Ashvin Vishwanath. Three-dimensional quantum spin liquids in models of harmonic-honeycomb iridates and phase diagram in an infinite- $D$  approximation. *Phys. Rev. B*, 90:205126, Nov 2014.
- [180] SungBin Lee, Eric Kin-Ho Lee, Arun Paramekanti, and Yong Baek Kim. Order-by-disorder and magnetic field response in the Heisenberg-Kitaev model on a hyperhoneycomb lattice. *Phys. Rev. B*, 89:014424, Jan 2014.
- [181] Eric Kin-Ho Lee and Yong Baek Kim. Theory of magnetic phase diagrams in hyperhoneycomb and harmonic-honeycomb iridates. *Phys. Rev. B*, 91:064407, Feb 2015.
- [182] A. Biffin, R. D. Johnson, Sungkyun Choi, F. Freund, S. Manni, A. Bombardi, P. Manuel, P. Gegenwart, and R. Coldea. Unconventional magnetic order on the hyperhoneycomb Kitaev lattice in  $\beta$ -Li<sub>2</sub>IrO<sub>3</sub>: Full solution via magnetic resonant x-ray diffraction. *Phys. Rev. B*, 90:205116, Nov 2014.
- [183] A. Biffin, R. D. Johnson, I. Kimchi, R. Morris, A. Bombardi, J. G. Analytis, A. Vishwanath, and R. Coldea. Noncoplanar and Counterrotating Incommensurate Magnetic Order Stabilized by Kitaev Interactions in  $\gamma$ -Li<sub>2</sub>IrO<sub>3</sub>. *Phys. Rev. Lett.*, 113:197201, Nov 2014.
- [184] Heung-Sik Kim, Eric Kin-Ho Lee, and Yong Baek Kim. Predominance of the Kitaev interaction in a three-dimensional honeycomb iridate: From ab initio to spin model. *EPL (Europhysics Letters)*, 112:67004, 2015.
- [185] Vamshi M. Katukuri, Ravi Yadav, Liviu Hozoi, Satoshi Nishimoto, and Jeroen van den Brink. The vicinity of hyper-honeycomb  $\beta$ -Li<sub>2</sub>IrO<sub>3</sub> to a three-dimensional Kitaev spin liquid state. *Scientific Reports*, 6:29585, Jul 2016.
- [186] Ying Li, Stephen M. Winter, Harald O. Jeschke, and Roser Valentí. Electronic excitations in  $\gamma$ -Li<sub>2</sub>IrO<sub>3</sub>. *Phys. Rev. B*, 95:045129, Jan 2017.
- [187] J. P. Hinton, S. Patankar, E. Thewalt, A. Ruiz, G. Lopez, N. Breznay, A. Vishwanath, J. Analytis, J. Orenstein, J. D. Koralek, and I. Kimchi. Photoexcited states of the harmonic honeycomb iridate  $\gamma$  - Li<sub>2</sub>IrO<sub>3</sub>. *Phys. Rev. B*, 92:115154, Sep 2015.
- [188] Itamar Kimchi and Radu Coldea. Spin dynamics of counterrotating Kitaev spirals via duality. *Phys. Rev. B*, 94:201110, Nov 2016.
- [189] A. Glamazda, P. Lemmens, S. H. Do, Y. S. Choi, and K. Y. Choi. Raman spectroscopic signature of fractionalized excitations in the harmonic-honeycomb iridates  $\beta$ - and  $\gamma$ -Li<sub>2</sub>IrO<sub>3</sub>. *Nature Communications*, 7:12286, 07 2016.

- [190] K. A. Modic, B. J. Ramshaw, Nicholas P. Breznay, James G. Analytis, Ross D. McDonald, and Arkady Shekhter. Robust spin correlations at high magnetic fields in the honeycomb iridates, preprint arXiv:1612.09410.
- [191] Heung-Sik Kim, Yong Baek Kim, and Hae-Young Kee. Revealing frustrated local moment model for pressurized hyperhoneycomb iridate: Paving the way toward a quantum spin liquid. *Phys. Rev. B*, 94:245127, Dec 2016.
- [192] Masahiko G. Yamada, Hiroyuki Fujita, and Masaki Oshikawa. Designing Kitaev spin liquids in metal-organic frameworks, preprint arXiv:1605.04471.
- [193] A. M. Cook, S. Matern, C. Hickey, A. A. Aczel, and A. Paramekanti. Spin-orbit coupled  $j_{\text{eff}} = 1/2$  iridium moments on the geometrically frustrated fcc lattice. *Phys. Rev. B*, 92:020417, Jul 2015.
- [194] A. A. Aczel, A. M. Cook, T. J. Williams, S. Calder, A. D. Christianson, G.-X. Cao, D. Mandrus, Yong-Baek Kim, and A. Paramekanti. Highly anisotropic exchange interactions of  $j_{\text{eff}} = \frac{1}{2}$  iridium moments on the fcc lattice in  $\text{La}_2\text{B}\text{IrO}_6$  ( $B = \text{Mg}, \text{Zn}$ ). *Phys. Rev. B*, 93:214426, Jun 2016.
- [195] Yoshihiko Okamoto, Minoru Nohara, Hiroko Aruga-Katori, and Hidenori Takagi. Spin-liquid state in the  $S=1/2$  hyperkagome antiferromagnet  $\text{Na}_4\text{Ir}_3\text{O}_8$ . *Phys. Rev. Lett.*, 99:137207, 2007.
- [196] Ryuichi Shindou. Nature of the possible magnetic phases in a frustrated hyperkagome iridate. *Phys. Rev. B*, 93:094419, Mar 2016.
- [197] Tomonari Mizoguchi, Kyusung Hwang, Eric Kin-Ho Lee, and Yong Baek Kim. Generic model for the hyperkagome iridate  $\text{Na}_4\text{Ir}_3\text{O}_8$  in the local-moment regime. *Phys. Rev. B*, 94:064416, Aug 2016.
- [198] Yongkang Luo, Chao Cao, Bingqi Si, Yuke Li, Jinke Bao, Hanjie Guo, Xiaojun Yang, Chenyi Shen, Chunmu Feng, Jianhui Dai, Guanghan Cao, and Zhu-an Xu.  $\text{Li}_2\text{RhO}_3$ : A spin-glassy relativistic Mott insulator. *Phys. Rev. B*, 87:161121, Apr 2013.
- [199] Chao Cao, Yongkang Luo, Zhuan Xu, and Jianhui Dai. Electronic structure of relativistic Mott insulator  $\text{Li}_2\text{RhO}_3$ , preprint arXiv:1303.4675.
- [200] P. Khuntia, S. Manni, F. R. Foronda, T. Lancaster, S. J. Blundell, P. Gegenwart, and M. Baenitz. Local Magnetism and Spin Dynamics of the Frustrated Honeycomb Rhodate  $\text{Li}_2\text{RhO}_3$ , preprint arXiv:1512.04904.
- [201] Turan Birol and Kristjan Haule.  $J_{\text{eff}} = 1/2$  Mott-Insulating State in Rh and Ir Fluorides. *Phys. Rev. Lett.*, 114:096403, Mar 2015.
- [202] Fei-Ye Li, Yao-Dong Li, Yue Yu, and Gang Chen. Kitaev materials beyond iridates: order by quantum disorder and Weyl magnons in rare-earth double perovskites, preprint arXiv:1607.05618.